January 2013

An Investigation Of Sub-Pixel Cloud/clear-Sky Contamination Using Hyper-Spectral AVIRIS Data

Celil Kaplan

AN INVESTIGATION OF SUB-PIXEL CLOUD/CLEAR-SKY CONTAMINATION USING HYPER-SPECTRAL AVIRIS DATA

by

Celil Kaplan

Bachelor of Engineering, Ankara University, 2010

A Thesis

Submitted to the Graduate Faculty

of the

University of North Dakota

In partial fulfillment of the requirements

for the degree of

Master of Science

Grand Forks, North Dakota
December
2013

This thesis, submitted by Celil Kaplan in partial fulfillment of the requirements for the Degree of Master of Science from the University of North Dakota, has been read by the Faculty Advisory Committee under whom the work has been done and is hereby approved.

Dr. Jianglong Zhang, Chairperson

Prof. Michael R. Poellot, Committee Member

Dr. Mark Askelson, Committee Member

This thesis is being submitted by the appointed advisory committee as having met all of the requirements of the School of Graduate Studies at the University of North Dakota and is hereby approved.

Dr. Wayne Swisher
Dean, School of Graduate Studies

December 2, 2013
Date

PERMISSION

Title An investigation of sub-pixel cloud/clear-sky contamination using hyper-spectral AVIRIS data

Department Atmospheric Sciences

Degree Master of Science

In presenting this thesis in partial fulfillment of the requirements for a graduate degree from the University of North Dakota, I agree that the library of this University shall make it freely available for inspection. I further agree that permission for extensive copying for scholarly purposes may be granted by the professor who supervised my thesis work or, in their absence, by the chairperson of the department or the dean of the School of Graduate Studies. It is understood that any copying or publication or other use of this thesis or part thereof for financial gain shall not be allowed without my written permission. It is also understood that due recognition shall be given to me and to the University of North Dakota in any scholarly use which may be made of any material in my thesis.

Celil Kaplan

11/26/2013

TABLE OF CONTENTS

LIST OF FIGURES…….....vii

LIST OF TABLES……..…ix

ACKNOWLEDGEMENTS……..x

ABSTRACT …….....xi

CHAPTER

I. INTRODUCTION …….……1

II. DATA AND METHODOLOGY …….....5

Hyper-spectral Imagery……..….5

Geostationary Satellite Observations…….……..…9

Cloud Detection……..……....15

Collocation and Comparison…….....18

Comparison of Theoretically and Empirically Derived Values….20

III. RESULTS AND DISCUSSION …….....23

Cloud Detection…….....23

Comparison of GOES IR and Visible Cloud Detection Methods..43

Comparison of GOES and AVIRIS Cloud Fraction…….....45

Uncertainty analysis…..……..…….....49

Modeled and Observed Radiance Values at the AVIRIS Spectrum……51

IV. SUMMARY AND CONCLUSIONS…….....56

APPENDIX……60

REFERENCES ……......62

LIST OF FIGURES

Figure Page

1. Flow diagram of the BTH technique……..…….…….....18

2. Comparison of dimensions of pixels from AVIRIS and GOES IR channels…….20

3. RGB AVIRIS image taken on 29 October, 2008 between 20:10 and 20:19 GMT, over the west coast of the northern California……..…….....25

4. GOES-11 images taken at 20:15 GMT 29 October, 2008 over the western US showing (a) Channel 1, (b) Channel 2, (c) Channel 3, (d) Channel 4, (e) Channel 5, and (f) a false color composite focused on the area of interest (black lines highlight the spatial coverage of the AVIRIS data, and pink, blue, and aquamarine colors represent cloud, ocean, and land areas respectively)….....26

5. All training pixels and their radiance values across the whole spectrum.….....…..28

6. Selected cloud, forest and ocean pixels and their respective radiance values throughout the AVIRIS spectrum…….…….....…29

7. (a) AVIRIS original image, (b) water-mask after the 2.28 μm channel test, and (c) water-mask after using both the 0.8 and 2.28 μm channel tests (black color indicates water)…….....30

8. (a) AVIRIS original image, (b) vegetation mask, and (c) thin cirrus mask (black color indicates vegetation in (b) and thin cirrus in (c))....32

9. (a) Original AVIRIS image and (b and c) the results of two enhancing tests (black color indicates masked areas by tests)…….....33

10. (a) Original AVIRIS image and (b) result of the combination of all tests (black color indicates masked areas by tests and purple color indicates thin cirrus).....34

11. Spectral responses of selected cloud and city pixels for the spectral range from 0.4 to 2.5 μm.……..…….....35

12. First derivative of radiance values respect to the wavelength…….....36

13. Second derivative of radiance values respect to the wavelength……...…36

14. (a) Original AVIRIS image, (b) black and white image showing cloudy, and non-cloudy areas, and (c) application of the land-mask to this image…….....38

15. (a) Original false color GOES and (b) corresponding $\Delta T_{10.7-3.9}$ images (black lines highlight the spatial coverage of the AVIRIS data)……..…..……...39

16. Results of the (a) first step, (b) second step, and (c) all steps of the BTH algorithm, and (d) original false color GOES image (black lines highlight the spatial coverage of the AVIRIS data)…….....40

17. GOES channel 1 image in the AVIRIS scan area and the detected cloudy GOES pixels (white color) using thresholds of (b) 5.5%, (c) 4.5%, and (d) 7.0%...….....43

18. (a) GOES pixels from Channel 2 in the AVIRIS scan area, (b) degraded Channel 1 pixels in that area, (c) resulting image after applying the BTH method, and (d) resulting image after applying the albedo method.……..….44

19. Comparison of the percentage of the cloudy areas in the infrared region…….....46

20. Comparison of the percentage of the cloudy areas in the visible region…….....47

21. GOES visible radiance as a function of AVIRIS cloud fraction, for GOES detected cloud free regions…….……47

22. Visible channel cloud mask (upper row) and infrared channels cloud mask (lower row) for GOES data from 20:00, 20:15, and 20:30 GMT, on 29 October, 2008 (from left to right, respectively)…….....50

23. AVIRIS and SBDART comparison over ocean for different types of aerosols (AVIRIS data are shown in red, and SBDART outputs are shown in purple, blue, green, and yellow for AOD=0, 0.1, 0.2, and 0.5, respectively)……..…...53

24. Radiance values for different aerosol models throughout the spectrum for and AOD of 0.5…….....54

25. Change in radiance values between the 0.7 and 0.8 μm channels with varying AOD when the tropospheric aerosol model is used…..……...…….....55

26. Change in radiance values between 0.9 and 1.2 μm channels with varying AOD when the oceanic aerosol model is used…….....55

LIST OF TABLES

Table Page

1. AVIRIS sensor characteristics……...……...6
2. Nominal AVIRIS Data Characteristics……..…..……..…….....7
3. Contents of an AVIRIS distribution tar file……..….....8
4. GOES-11-Imager specifications……..…..…….....12
5. GOES-11-Imager scaling coefficients for radiance conversion…….....14
6. GOES-11-Imager scaling coefficients for temperature conversion.……...15
7. Effect of sub-pixel cloud/clear-sky contamination in measured GOES radiance (Rad.) and temperature (Temp.) values. (Radiance values are in μW cm^{-2} nm^{-1} sr^{-1} and temperature values are in Kelvin, and percentages in parenthesis after values represent increases/decreases in value).…….....…….....48
8. Sub-pixel cloud and clear-sky contamination for four simulated GOES datasets. The four GOES datasets were created by arbitrarily shifting the GOES pixels one pixel away from their original location, either to the left or to the right, or up or down...…….…….....51

ACKNOWLEDGEMENTS

Thank you to my advising committee of Drs. Jianglong Zhang and Mark Askelson, and Prof. Michael R. Poellot for their continual guidance and support throughout the course of this thesis work. Thank you to all of my family and friends for their encouragement, love, and support. Thank you to all of the graduate students in the Atmospheric Sciences Department for the fun times during my graduate school experience, especially those in my research group.

ABSTRACT

Cloud and clear sky contamination due to sub-pixel clouds remains as a troubling issue for scientific applications that rely on remotely sensed data. Sub-pixel level clouds may not be detected by a standard cloud filtering process, and thus can cause uncertainties in satellite–based meteorological property retrievals. In this study, using collocated data from Airborne Visible/Infrared Imaging Spectrometer (AVIRIS) and Geostationary Operational Environmental Satellite (GOES) data, sub-pixel cloud and clear-sky contamination were studied over the west coast of Northern California. The hyper-spectral data from AVIRIS have a spatial resolution on the order of 11.5 m for the study case, thus can be used for carefully examining the sub pixel cloud related bias in GOES data. This study suggest that significant sub-pixel cloud and clear-sky contamination exist, and should be considered for future applications that use measurements from passive sensors such as GOES. Lastly, simulated AVIRIS radiance values from a radiative transfer model were used to explore the possibility of using AVIRIS data for future aerosol studies.

CHAPTER I

INTRODUCTION

Clouds that originate from both dynamic and thermodynamic processes in the atmosphere play an important role in both climate and weather related studies (Hawkinson et al. 2005). Clouds reflect solar energy while absorbing terrestrial longwave emissions, thus they have both warming and cooling effects on the earth-atmospheric system. The signs of cloud climate effects are highly dependent upon cloud optical and physical properties. The modification of cloud properties with changes in aerosol concentrations and properties, known as the aerosol indirect effect, remains as the largest uncertainty in climate studies (IPCC, 2011). Equally important is the understanding of cloud properties for weather related applications. For example, weather events such as tornadoes and hail storms are detrimental to regional economic activities and are always accompanied by cloud systems that can be used to infer meteorological conditions of the surrounding areas. With this knowledge, the damages may be reduced by improving forecasting accuracies through a better understanding of the physical and optical properties of clouds. Clearly, the study of cloud optical properties (e.g., optical depth, effective radius, single scattering albedo, and phase function) and physical properties (e.g., cloud cover, cloud top height, thickness, water content and sizes of droplets or ice crystals) is critical to both climate and weather applications.

Previous studies have observed cloud properties through *in situ* measurements and by using ground and space-based remote sensing techniques. *In situ* studies include the

direct sampling of cloud properties such as droplet size distributions using aircraft measurements (e.g. Evans et al. 2003). However, *in situ* measurements are rather costly and are spatially and temporarily limited. Ground-based radar measurements can be used to study three dimensional cloud optical properties at a high temporal resolution (e.g. Miller et al. 1998). However, the spatial coverage of radar data is limited as well, especially for analysis at a global scale or over oceans. In comparison, satellites, especially polar orbiting satellites, can be used to observe the Earth and atmospheric system with near global coverage on a daily basis. As a result, measurements from satellites have been widely used to study cloud properties on both global and regional scales.

Satellite observations, however, also have limitations when used for cloud studies. For example, one of the major issues for satellite based cloud studies is spatial-sampling-related bias such as sub-pixel cloud contamination. Smaller clouds often have spatial coverage less than a pixel size of a satellite image, and which could result in a pixel being misidentified as cloud free. Sub-pixel cloud contamination is an issue for satellite remote sensing, as the pixels with sub-pixel clouds have different optical properties than those that are cloud free. Uncertainties and biases appear when used in the clear-sky retrieval methods and in studies involving chemical species and aerosol property retrievals. Conversely, uncertainties also exist for cloud property retrievals over partially clouded regions that are misclassified as cloudy pixels (sub-pixel clear-sky contamination). Sub-pixel cloud/clear-sky contamination, however, has not been widely studied for its impacts on applications such as aerosol retrievals, and such a topic deserves further exploration, possibly using collocated observations with different spatial resolutions.

It is clear that instruments that provide very high spatial resolution measurements are needed for studying sub-pixel cloud/clear-sky contamination. Fortunately, airborne hyper-spectral instruments such as Airborne Visible/Infrared Imaging Spectrometer (AVIRIS) have spatial resolutions on the order of 10 m, and can be used to investigate sub-pixel cloud/clear-sky contamination in multi-spectral satellite observations. This study uses collated AVIRIS and Geostationary Operational Environmental Satellite (GOES) data to study sub-pixel cloud/clear-sky contamination. A threshold based cloud screening method is developed for cloud-screening of AVIRIS data, and cloud fields detected by AVIRIS are inter-compared with the collocated GOES data.

GOES data were selected for this study for multiple reasons. First, only one AVIRIS granule is available in order to perform this sub-pixel cloud study, and only the GOES-11 satellite has near simultaneous observations at the AVIRIS overpass. Second, GOES satellites, due to their high temporal and spatial resolution, have been widely used for both weather forecasts and scientific research. Finally, there are no polar orbiting satellites that coincide with AVIRIS data.

Since its introduction, several cloud detection algorithms have been developed for the GOES data. The most common GOES cloud screening method was developed by Jedlovec and Laws (2003). The method (i.e., the bi-spectral threshold and height (BTH) method) uses spatially and temporally varying thresholds to identify clouds in the GOES dataset. The basic principle of this method is that the emissivity difference of clouds at 10.7 μm and 3.9 μm channels varies from that of the surface (land or ocean) so that brightness temperature differences from these channels can then be used to detect the cloudy areas. The BTH method has been shown to produce better results than any other

GOES cloud screening methods especially during sunrise/sunset and at night (Jedlovec and Laws, 2003). In addition to the BTH method which uses infrared channels, some thresholds were determined for cloud detection at the visible channel (0.65 μm).

A new threshold based method is applied to the AVIRIS data and inter-compared with the collocated GOES data in order to investigate sub-pixel cloud/clear-sky contamination in GOES data. In addition, radiative transfer model (RTM) calculations are used to simulate AVIRIS data in order to study the impacts of aerosols on observations from hyper-spectral sensors such as AVIRIS for future aerosol related applications. The intent is to address the following scientific questions in this thesis:

(1) what are the percentages of the sub-pixel cloud cover when pixels marked as clear/cloudy by the GOES cloud mask algorithm, and

(2) which channels of the AVIRIS spectrum may be useful for use in a future cloud/aerosol detection algorithm?

CHAPTER II

DATA AND METHODOLOGY

Hyper-spectral Imagery

The first goal of this study is to examine sub-pixel cloud/clear-sky contamination in GOES data using collocated AVIRIS data. The study of sub-pixel features in coarse resolution data using high resolution imagery is not new. For example, Morisette et al. (2003) used high spatial resolution IKONOS data for validating the Moderate Resolution Imaging Spectroradiometer (MODIS) land products; such as vegetation indices, leaf area indices, net primary vegetation production, and variations in land cover. The Multispectral Thermal Imager (MTI) has been applied to evaluation of effects of spatial resolution on the accuracy of aerosol optical depth retrievals by Henderson et al. (2005). Chylek et al. (2004) used MTI data to study the effect of broken clouds on satellite-based retrievals of column water vapor concentration. Yet, no attempt has been made to study sub-pixel cloud/clear sky contamination using hyper-spectral measurements from airborne sensors such as AVIRIS for cloud and aerosol property retrievals.

Designed in 1983, AVIRIS has been used for observing the earth and atmospheric system since 1987 (Green et al. 1998). The instrument is mounted on an aircraft, which flies approximately 20 km above the surface of the Earth. Each year, AVIRIS scans over different areas in the USA, Canada and Europe. The flight schedules are managed by the National Aeronautics and Space Administration (NASA) Jet Propulsion Laboratory (JPL) (AVIRIS overview 2013).

AVIRIS has a complex optical sensor consisting of a number of major subsystems, components and characteristics (Green et al. 1998). As shown in Table 1, it has a cross-track (sweeps back and forth) scanner with 224 detectors. The sensor receives white light in the fore-optics, spectrally disperses the light, converts photons to electrons, amplifies the signal, digitizes the signal, and records the data to a high density tape (Green et al. 1998). Table 2 shows some data characteristics of the instrument. The 224 channels are contiguous, with a spectral bandwidth of approximately 10 nm, allowing it to cover the entire spectral range between 0.4 and 2.5 μm.

Table 1. AVIRIS sensor characteristics (Green et al. 1998).

Imager type	Whiskbroom scanner
Scan rate	12 Hz
Dispersion	Four grating spectrometers (A,B,C,D)
Detectors	224 detectors (32, 64, 64, 64) Si and InSb
Digitization	12 bits
Data rate	20.4 Mbits/s
Spectrum rate	7300 spectra/s
Data capacity	>10 GB (>8000 km²)

AVIRIS data have to be calibrated spectrally, radiometrically, and spatially in order to get physical parameters from measured radiance (Green et al. 1998). Thus, data can be compared with retrievals acquired using other instruments, and also computer model output (Green et al. 1998). These calibrations are applied before and after each flight in a laboratory (Chrien et al. 1995b). When spectrally calibrating the instrument, calibrated monochromator input and AVIRIS signals are analyzed to determine the uncertainties of the 224 spectral bands (Chrien and Green, 1993). Radiometric calibration

is done through determining the radiometric calibration coefficients, which are calculated using the ratio of the known radiance incident at AVIRIS and the digitized numbers reported by AVIRIS. Spatial calibration is done periodically in a manner similar to spectral calibration (Chrien and Green, 1993). During this calibration, spatial response functions are calculated for examining targets having dimensions near or below AVIRIS spatial resolution (Green et al. 1998).

Table 2. Nominal AVIRIS Data Characteristics (Green et al. 1998).

Spectral	
Wavelength range	0.4-2.5 µm
Sampling	0.01 µm
Spectral response (FWHM)	0.01 µm
Calibration accuracy	<0.001 µm
Radiometric	
Radiometric range	0 to maximum Lambertian radiance
Sampling	~1 Data Number (DN) noise Root Mean Square (RMS)
Absolute calibration	≥96%
Inter flight stability	≥98%
Signal-to-noise	Exceeding 100:1 requirement
Polarization sensitivity	≤ 1%
Spatial (at 20 km altitude)	
Field of view (FOV)	30 degrees (11 km)
Instantaneous FOV	1.0 mrad (20 m)
Calibration accuracy	≤0.1 mrad
Flight line length	800 km total

Each AVIRIS dataset comes with a set of files shown in Table 3; several of which were used in this study. In particular, the '*.gain' file contains coefficients for converting dimensionless digital numbers into radiance values. When values in a spectrum are divided by the coefficient in this file, the 16-bit integers are converted into radiance values (units of µW cm^{-2} nm^{-1} sr^{-1}). The '*_obs_ort' file includes: path length (sensor-to-ground in meters); to-sensor-azimuth (0 to 360 degrees clockwise (cw) from N); to-sensor-zenith (0 to 90 degrees from zenith); to-sun-azimuth; to-sun-zenith; phase

(degrees between to-sensor and to-sun vectors in the principal plane); slope (local surface slope as derived from digital elevation model (DEM) in degrees); aspect (local surface aspect 0 to 360 degrees cw from N); cosine i (apparent local illumination factor based on DEM slope and aspect and to-sun vector, -1 to 1) and Greenwich Mean Time (GMT) time (decimal hours for mid-line pixels). The geometry file (*_ort_igm) contains the longitude, latitude and elevation at each pixel center. Lastly, the image file (*_ort_img) contains the AVIRIS calibrated radiances multiplied by the gain and are stored as 16-bit integers.

Table 3. Contents of an AVIRIS distribution tar file.

*.info	General information about the flight line
*.gain	Multiplication factors, radiance to 16-bit integer
*.geo	Geometric calibration data
*.rcc	Radiometric calibration coefficients
*.spc	Spectral calibration file
*_eph	Position data in a World Geodetic System (WGS)-84/North America Datum (NAD)83 Universal Transverse Mercator (UTM) x,y,z coordinate system
*_lonlat_eph	Position in WGS-84 longitude, latitude and elevation
*_obs	Pertinent parameters relating to the geometry of the observation and illumination conditions before the geometric look up table (GLT) applied
*_obs_ort	Pertinent parameters relating to the geometry of the observation and illumination conditions after the GLT applied
*_ort_glt	Orthocorrected GLT file
*_ort_igm	Orthocorrected input geometry file
*_ort_img	Calibrated AVIRIS radiance (image) data

The AVIRIS dataset used in this research was collected over Monterrey Bay, CA on 29 October 2008 between 20:10 and 20:19 GMT. An ER-2 high-altitude airborne science aircraft was flown at 122.05ºW longitude and latitude ranging from 36.55ºN to 36.98ºN. The average altitude of the aircraft was 13.7 km, at which the AVIRIS data have

a spatial resolution of 11.5 m. Both cloudy and cloud-free scenes are included in the AVIRIS granule (data).

AVIRIS image data files consist of 16-bit signed integers. These integers are lined up in a band interleaved by pixel (BIP) format (channel, sample, line). Thus, a conversion is needed wherein the multiplication factors stored in the gain file are applied to the 16-bit integers in order to convert them into radiance values, which are needed for this study. In the next step, radiometric correction steps were applied using the radiometric calibration and the spectral calibration files included in the AVIRIS data. The radiometric calibration file consists of the radiometric calibration coefficient and laboratory calibration uncertainty for each channel. The spectral calibration file consists of a wavelength center position, full width at half maximum (FWHM) for equivalent Gaussian, uncertainty in wavelength center position, and uncertainty in FWHM for equivalent Gaussian for each channel. Lastly, geometric correction was applied using the geometric calibration file. The geometric calibration file consists of a spatial sampling interval (pixel center to center distance on the ground, in milliradians), spatial response function, spatial sampling interval uncertainty (in milliradians), and spatial response function uncertainty (in milliradians) for each channel. The FWHM (in milliradians) of the spatial response function is also assumed to be Gaussian and is a measure of the nominal pixel size.

Geostationary Satellite Observations

National Oceanic and Atmospheric Administration (NOAA) geostationary satellites play an important role in observing variations in surface and atmospheric features over much of North America and the surrounding regions (Jedlovec and Laws,

2003). Since 1975, a total of 15 GOES satellites have been sent into space. The continuous viewing of the GOES-East and West satellites makes them useful in monitoring rapid changes in land surface temperature, atmospheric stability and clouds that are very important when monitoring short-term weather (Jedlovec and Laws, 2003). Though they have a lower spatial resolution when compared to most of the current low-earth orbiting (LEO) satellites such as MODIS, GOES imager and sounder products are widely used by NOAA, Department of Defense (DOD), NASA, and other agencies and private companies (Jedlovec and Laws, 2003). The GOES-Imager is a five channel (one visible, four infrared) imaging radiometer designed to sense radiant and solar reflected energy from sampled areas of the earth (GOES Imager Instrument 2013). In contrast, the GOES-Sounder is a nineteen channel (one visible, eighteen infrared) radiometer that is specifically used for sensing atmospheric temperature and moisture profiles, surface and cloud top temperatures, and ozone distribution (GOES Sounder Instrument 2013).

The on-board radiometric calibration is included for the GOES infrared channels (Weinreb et al. 1997). The radiometric calibration of the GOES-Imager is done by first pointing the sensor to space for roughly 2.2 seconds, and then pointing the sensor to an internal blackbody with known temperature of 300 K (GOES N Series Data Book 2009). No on-board calibration, however, is included for the GOES visible channel (Weinreb et al. 1997) Therefore, external calibration steps are needed to account for any signal degradation and for using the GOES visible channel in property retrievals. The accuracy of the system is less than or equal to 1 K for infrared channels and 5% of maximum scene irradiance for the visible channel (GOES Sounder Instrument 2013).

Users of GOES datasets receive scaled radiances in a GOES variable format (GVAR) data stream. The data from the channels of the imagers and sounders are scaled in 16 bit words. Coefficients are needed to convert the 16 bit words into radiances and can vary by both satellite and detector. The Planck function is further used to convert radiances to effective temperatures. In the final step, effective temperatures are converted into actual temperatures.

On the date of the AVIRIS scan, both GOES-11 and 12 data are available. The GOES-11 and 12 satellites provide GOES-West and East retrievals, respectively. Because of the location of the AVIRIS scan, GOES-11 is chosen for this research. The specifications of the GOES-11-Imager are provided in Table 4, which shows the spatial resolutions of GOES-11 visible and infrared channels to be 1 km and 4 km (as nominal squares), respectively. While Channel 1 is the only channel in the visible spectrum, GOES has four different channels devoted to the infrared region. According to the wavelength ranges in Table 4 these infrared channels can be described as middle infrared, water vapor and two thermal infrared channels. The range of the GOES measurements and meteorological objectives of each channel are also shown in Table 4. In the visible spectrum, GOES is sensitive to albedo values between 1.6 and 100% and so the visible channel is useful to assess cloud cover. On the other hand; in the infrared region, it is sensitive to temperatures between approximately 180 and 330 K. Cloud detection algorithms use these infrared channels, as temperature is more essential than albedo to discriminating clouds from rest of the features.

Table 4. GOES-11-Imager specifications (GOES Imager Instrument 2013).

Channel Number	Nominal Square IGFOV at Nadir	Wavelength Range (μm)	Range of Measurement	Meteorological Objective and Maximum Temperature Range
1	1 km	0.55 to 0.75	1.6 to 100% albedo	Cloud Cover
2	4 km	3.80 to 4.00	180 to 335 K	Nighttime clouds (space-340K)
3	4 km	6.50 to 7.00	180 to 329 K	Water vapor (space-290K)
4	4 km	10.20 to 11.20	180 to 329 K	Sea surface temperature and water vapor (space to 335K)
5	4 km	11.50 to 12.50	180 to 329 K	Sea surface temperature and water vapor (space to 335K)

A conversion is needed for translating GOES data into radiance/temperature values. Since there is no on-board calibration for the GOES visible channel, the calibration coefficients are also applied to the GVAR data stream (Weinreb et al. 2009). The calibration equation is

$$R = mX + b \,, \qquad (1)$$

where X is the instrument output in GVAR counts and m and b are the calibration coefficients measured before launch. The radiance, R, is the average of the spectral (monochromatic) radiance over the spectral response function for that visible detector in units of W m^{-2} sr^{-1} μm^{-1} (Weinreb et al. 2009). The measured m and b values for 10-bit GVAR counts of GOES-11 are 5.561568×10^{-1} W m^{-2} sr^{-1} μm^{-1} $count^{-1}$ and -16.129 W m^{-2} sr^{-1} μm^{-1}, respectively (Weinreb et al. 2009). These values are constant for each GOES satellite, and do not vary by time. When converting 16-bit into 10-bit, the GVAR counts need to be divided by 32. The value of b in (1) is calculated using

$$b=-mX_0\ , \qquad (2)$$

where m here is the slope for the reference detector and X_0 is a reference value for the GOES visible channel and is dimensionless (set to a value of 29 (Weinreb et al. 2009)). To convert radiance values into albedo values, radiance values were simply multiplied by 2.01524×10^{-3} (Weinreb et al. 2011). This value is determined through the ratio of maximum albedo and radiance values that GOES can measure (1.0 and 500 W m^{-2} sr^{-1} μm^{-1}, respectively). It is noted that although the GOES visible channel suffers from signal degradation (Zhang et al., 2001), no correction is implemented for the decrease in radiance values in the GOES visible channel with respect to time. This is because only one GOES granule is used in this study, and the signal degradation can be accounted for by lowering the cloud detection thresholds.

No external calibration step is needed for the GOES IR channels due to the existing on-board calibration. The conversion algorithm starts with first converting the 10-bit GVAR counts into radiances and then into temperature values. A 10-bit GVAR count is converted to a scene radiance according to

$$R=\frac{(X-b)}{m}\ , \qquad (3)$$

where R is radiance and X is the GVAR count value (Weinreb et al. 2009). Note that both equation 1 and 3 are linear, but the forms are different for calculation purposes. The coefficients m and b are the scaling slope and intercept, respectively, and are given in Table 5.

Table 5. GOES-11-Imager scaling coefficients for radiance conversion (Weinreb et al. 2011).

Channel	m	b
2	227.3889	68.2167
3	38.8383	29.1287
4	5.2285	15.6854
5	5.0273	15.3332

To convert the scaled radiance to effective temperature, the Planck function is used:

$$T_{eff} = \frac{c_2 * v}{\ln[1 + (c_1 * v^3)/R]}, \quad (4)$$

where T_{eff} is the effective temperature (K), and R is the radiance. The coefficient v is the central wavenumber of the channel, which is dependent upon on the spectral characteristics of a channel while c_1 (1.191066×10^{-5}) and c_2 (1.438833) are the two radiation constants, respectively (Weinreb et al. 2009). "The central wavenumber for a detector is defined to be that wavenumber that splits the area under the spectral response function (SRF) into two equal halves" (Weinreb et al. 2009). The values of v are listed in Table 6. Lastly, the effective temperatures are inverted to actual temperatures using

$$T = \propto + \beta * T_{eff}, \quad (5)$$

where α and β are two conversion coefficients and are listed in Table 6. These two coefficients are determined through comparing known actual temperature values with effective temperature values of several pixels (Weinreb et al. 2009).

Table 6. GOES-11-Imager scaling coefficients for temperature conversion (Weinreb et al. 2011).

Channel	v	α	β
2	2562.07	-0.644790	1.000775
3	1481.53	-0.543401	1.001495
4	931.76	-0.306809	1.001274
5	833.67	-0.333216	1.001000

Cloud Detection

AVIRIS data include observations over a spectrum ranging from 0.4 to 2.5 μm, with a spectral interval of 0.01 μm. Discriminating cloudy areas from other surface features can thus be approached through examining radiance values over the entire AVIRIS spectrum. Since very few studies have investigated the cloud-clearing of AVIRIS data, a new threshold-based method is attempted for masking cloudy AVIRIS pixels. The new threshold method is based upon learning the spectral behaviors of scenes such as optically thin and thick clouds, thin cirrus clouds, vegetation, soil and ocean using preselected training samples. The spectral behavior of each selected scene is studied over the full spectral range of 0.4-2.5 μm. Spectra that are most sensitive to the presence of clouds are selected for cloud screening of AVIRIS data.

GOES cloud masking is accomplished by commonly used BTH method. This method uses the temperature differences between Channels 2 and 4. During the day light hours, this difference is determined to be a largely negative in the presence of clouds (Jedlovec and Laws, 2003). The four datasets that are used in the BTH method include: (1) the differences between GOES Channel 2 and 4; a multi-day composite representing the (2) smallest negative and (3) smallest positive differences (values closest to zero) from the preceding 20 day period; and (4) a 20 day composite generated using the highest

long-wave (10.7 μm) temperature for each location (pixel) from the preceding 20 day period (Jedlovec and Laws, 2003).

Using the four datasets described above, four steps are taken in the BTH algorithm for cloud screening of GOES data (Fig. 1). The first step, the adjacent pixel test, uses the first dataset (1) described in the preceding paragraph. According to this step, each pixel (i) along the scan line of GOES data is compared to the previous one (i-1). If the difference in adjacent pixels is greater than 27.4 K, then pixel i is marked as a cloud edge (Jedlovec and Laws, 2003). The second step, the one-dimensional spatial variability test, attempts to detect cloudy pixels around the cloud edges (Jedlovec and Laws, 2003). For a pixel to be marked as cloudy, the difference between pixels i and i-1 in the first dataset has to be less than 0 K if pixel i-1 is marked as cloudy in the previous step, or it must be less than -3 K if pixel i-1 is clear. The third step, the minimum difference test, compares the current difference image value (dataset 1) to the largest negative (dataset 2) and smallest positive (dataset 3) difference image values (Jedlovec and Laws, 2003). If the current difference image value is negative and the difference between the current difference image value and the largest negative difference image value is greater than 5.1 K, then the pixel is deemed to be cloudy. On the other hand, if the current difference image value is positive and the difference between the current difference image value and the largest positive difference image value is greater than 2 K, then the pixel is deemed to be cloudy. The fourth step, the infrared threshold test, utilizes the 10.7 μm channel information to catch a few clouds missed by the previous steps (Jedlovec and Laws, 2003). For a cloud to be detected, the value of the 10.7 μm channel of the current image

has to be 18.5 K colder than the warm 10.7 μm channel composite image (dataset 4) for that location.

A second method, based on GOES visible channel retrievals, was also implemented for comparison purposes. This method was developed by Jedlovec et al. (2009) to enable use of the visible channel in GOES cloud detection algorithms. In order to use this method, GVAR counts are converted into radiance values. These values are then converted into reflectance (albedo) values using the calibration method described in the previous section. Clouds appear brighter than the other surface types (ocean, vegetation, soil) in the visible spectrum, which in turn results in higher albedo values. Using this relationship, Jedlovec et al. (2009) determined the albedo thresholds as 7% over ocean and 25% over land. Values greater than these thresholds denote regions dominated by clouds in GOES datasets.

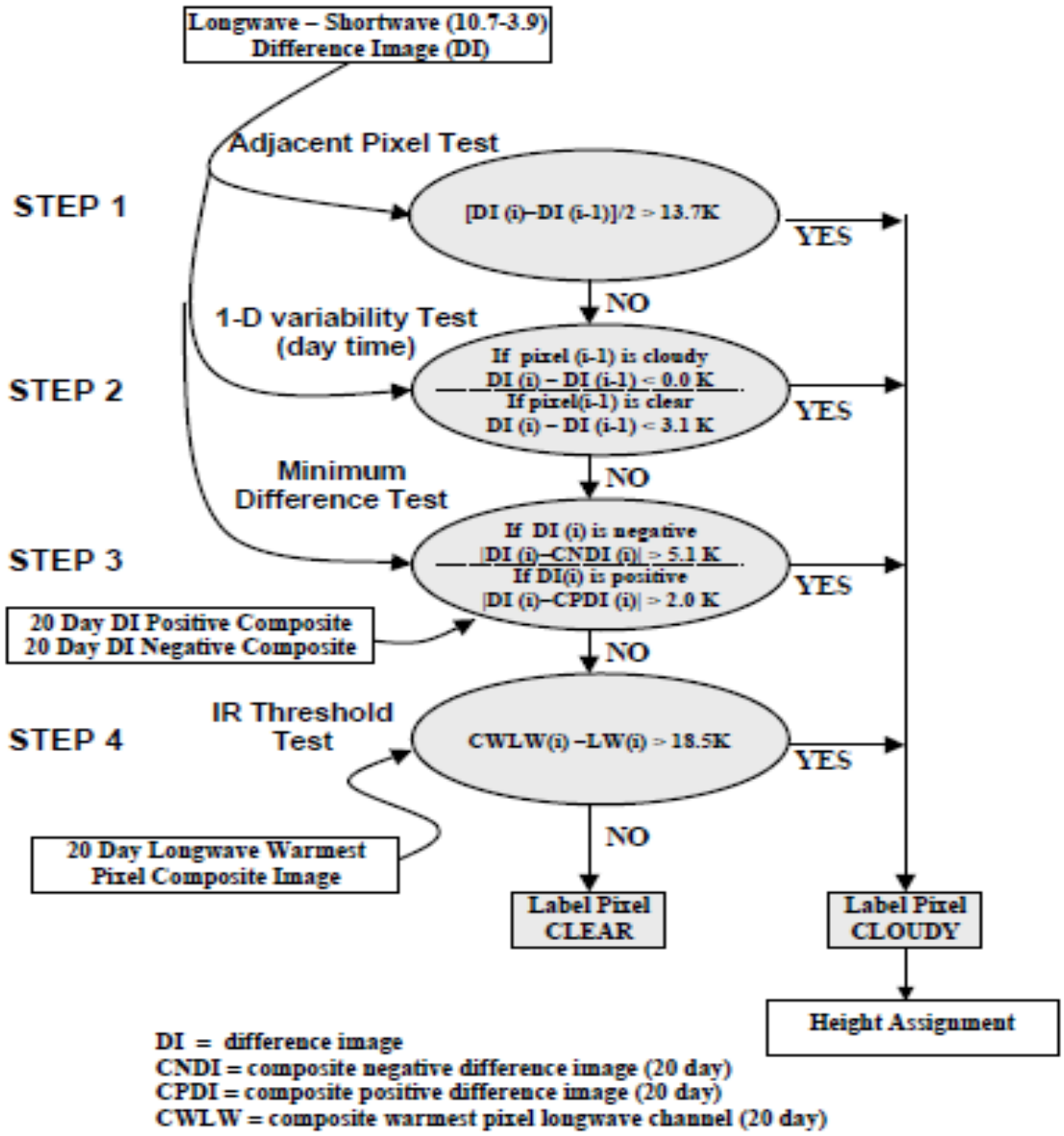

Figure 1. Flow diagram of the BTH technique (Jedlovec and Laws 2003).

Collocation and Comparison

To study sub-pixel cloud/clear-sky contamination within the GOES and AVIRIS datasets, observations from the two sensors need to be collocated in both space and time. To collocate the two datasets temporally, one GOES 11 granule that is within the overpassing times of the AVIRIS platform is selected. Spatial collocation is

accomplished by selecting AVIRIS pixels that are within the footprint of a GOES pixel. A nominal comparison of their spatial resolutions (GOES IR channels versus AVIRIS) is shown in Fig. 2. To collocate two pixels, first, GOES pixels that fall within the AVIRIS scan area are selected. Next, for such a GOES pixel, AVIRIS pixels that are within the footprint of the GOES pixel are identified. It is noted that some AVIRIS pixels can be labeled as "bad". Therefore, if a GOES pixel contains more than 50% of these collocated AVIRIS pixels, it is excluded from the study.

The process begins by comparing the two GOES cloud detection methods (the BTH and albedo-based method) pixel-by-pixel. In this comparison the spatial resolution of the visible channel (1 km) is degraded to 4 km (nominal) using geo-coordinates of each pixel. Then these pixels are compared as being cloudy or clear, according to the results of the cloud detection methods. Next, using collocated AVIRIS and GOES data, the average cloud fractions in GOES cloudy and clear scenes are calculated based upon AVIRIS data. In this step, each GOES pixel is located in the AVIRIS data. Then, the real cloud fraction acquired from the results of the AVIRIS cloud detection is compared to the GOES cloudy and clear pixels. The comparison is performed separately for different GOES cloud detection methods, as the spatial resolutions are different.

Finally, effects of sub-pixel cloud/clear-sky contamination on radiation/temperature values are investigated. In this step, the radiance/temperature values of GOES cloudy pixels (defined as the "true cloudy", determined by the albedo/BTH tests), which have the highest AVIRIS cloud fraction (determined by the AVIRIS), are determined and averaged. Then, radiance/temperature values of all GOES cloudy pixels are averaged. The difference between the averaged value from "true

cloudy" GOES pixels and the averaged value from all cloudy GOES pixels is used to represent the sub-pixel clear sky contamination. Similarly, radiance/temperature values of "true" GOES clear-sky pixels (as determined by both AVIRIS and GOES data) are determined and averaged. Then, radiance/temperature values of all GOES clear-sky pixels are averaged. The sub-pixel cloud contamination is defined as the difference between the averaged from all GOES "true" clear pixels and the averaged value from all GOES clear sky pixels.

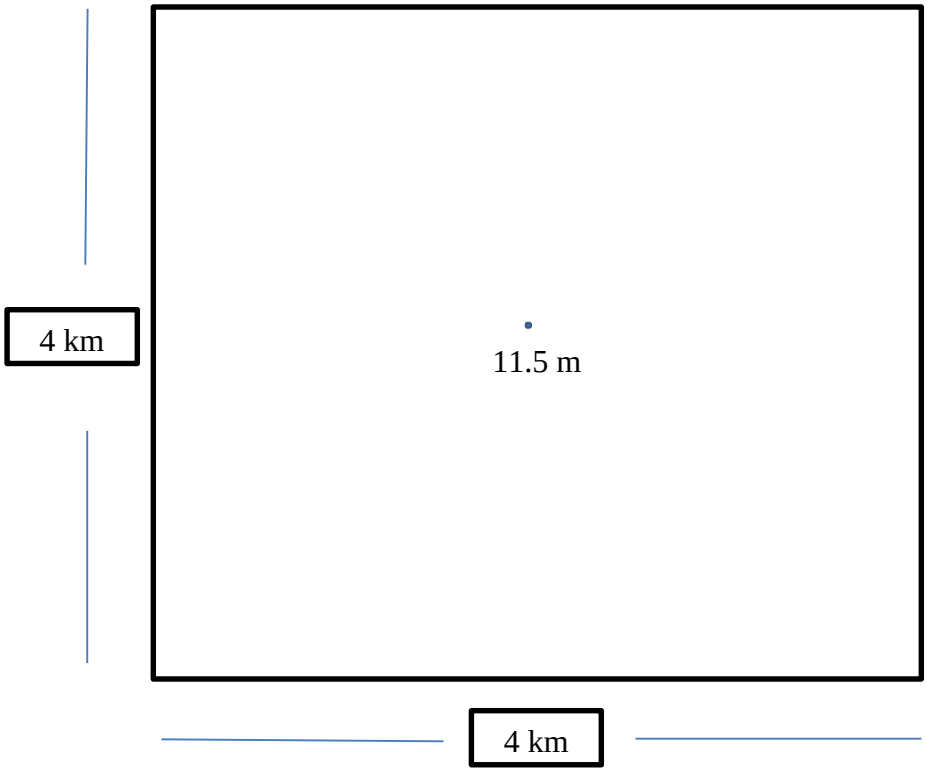

Figure 2. Comparison of dimensions of pixels from AVIRIS and GOES IR channels.

Comparison of Theoretically and Empirically Derived Values

To aid development of the AVIRIS cloud mask and to explore the use of hyper-spectral data for future aerosol related studies, the observed AVIRIS radiance values across the 0.4-2.5 μm spectrum are also compared with radiance values computed using Santa Barbara Discrete ordinate method (DISORT) Atmospheric Radiative Transfer

(SBDART) model. "SBDART is a FORTRAN computer code designed for the analysis of a variety of radiative transfer problems encountered in studies involving satellite remote sensing and the atmospheric energy budget" (Ricchiazzi et al. 1997). The code is a combination of an advanced DISORT model, low-resolution atmospheric transmission models, and Mie scattering results for light scattering by water droplets and ice crystals (e.g. Ricchiazzi et al. 1997). SBDART uses well-tested and reliable physical models that have been developed by the atmospheric science community over the past few decades (e.g., Ricchiazzi et al. 1997). Some key components of the program include cloud models, gas absorption models, extraterrestrial source spectra, standard atmospheric models, standard aerosol models, an RT equation solver, and surface models.

In particular, the LOWTRAN 7 atmospheric transmission model (e.g. Pierluissi et al. 1987) is included in SBDART for estimating gas absorption. The LOWTRAN 7 atmospheric transmission model was derived from detailed line-by-line calculations and includes the effects of all optically active molecular species found in the Earth's atmosphere. Six standard atmospheric models are used in SBDART for typical climatic conditions: tropical, mid-latitude summer, mid-latitude winter, subarctic summer, and subarctic winter. These models are widely used in the atmospheric research community for standard atmospheric conditions. SBDART can be used to compute the radiative effects of some common boundary layer and upper atmospheric aerosol types (e.g., rural, urban, maritime, volcanic, meteoric, etc.). As a RT equation solver; SBDART uses DISORT (Stamnes et al. 1988), which provides a numerically stable algorithm to solve the equations of plane-parallel RT in a vertically inhomogeneous atmosphere. Finally, six basic surface types are used to parameterize the spectral reflectivity of the surface: clear

water, lake water, sea water, vegetation, snow, and sand. In this study, radiance values computed from SBDART are compared with AVIRIS observations collected over the open ocean. The sensitivities of AVIRIS data to changes in aerosol concentration and aerosol type are also explored.

CHAPTER III

RESULTS AND DISCUSSION

Cloud Detection

Figure 3 shows the RGB image generated using observations from AVIRIS data at the 0.453, 0.55, and 0.821 μm channels as blue, green, and red colors respectively. The AVIRIS image is geo-rectified. However, the spatial coverage of the image is less than one degree on a latitude/longitude spatial grid and, therefore, the image is not plotted against a map. The land and ocean areas as shown in Figure 3 represent a small portion of west coast of northern California (upper part of the image) and the Pacific Ocean (lower part of the image) adjacent to the coast, respectively. Over the ocean region of the image, cumulus clouds are clearly visible. Note that the pixel size is on the order of 11.5 m and, therefore, some of the clouds have a size much less than 1 km (e.g., the approximate pixel size of the GOES visible channel). Thus, this is an ideal case for studying sub-pixel cloud/clear-sky contamination in GOES data.

Correspondingly, Figure 4 shows the black and white images from all five channels of the GOES-11 data as well as a zoomed in false-color composite. At the visible channel (Fig. 4a), ocean and land surfaces are clearly separable as ocean pixels are relatively dark compared to the pixels over land. In addition, stratocumulus clouds are visible over the west coast of the northern California. Bright clouds, which are observable over the bottom and upper left corner of Figure 4a, appear dark in the IR images (Figs.

4b-e). Figures 4b, 4d, and 4e show the temperatures of the observed scenes for GOES-11 channels 2, 4 and 5 respectively. Figure 4c (for GOES-11 channel 3) shows the water vapor features observed at the water vapor absorbing channel. GOES IR channels (Figs. 4b-e) confirm that these bright clouds are indeed high clouds, indicated by lower IR temperatures compared to surrounding areas. The stratocumulus clouds over the west coast of the northern California (region of hyper-spectral observations from AVIRIS), however, are not apparent in the IR images, suggesting the clouds over the study area are warm, near surface (~below 2 km) clouds. A false color composite (Fig. 4f) is also created, with a focus over the study area, using spatially degraded GOES-11 data from channels 1, 2, and 3. As illustrated in Figure 4f, stratocumulus clouds are observed over the ocean but not over land, and the stratocumulus clouds extend along and near the coastline over the northern part of California.

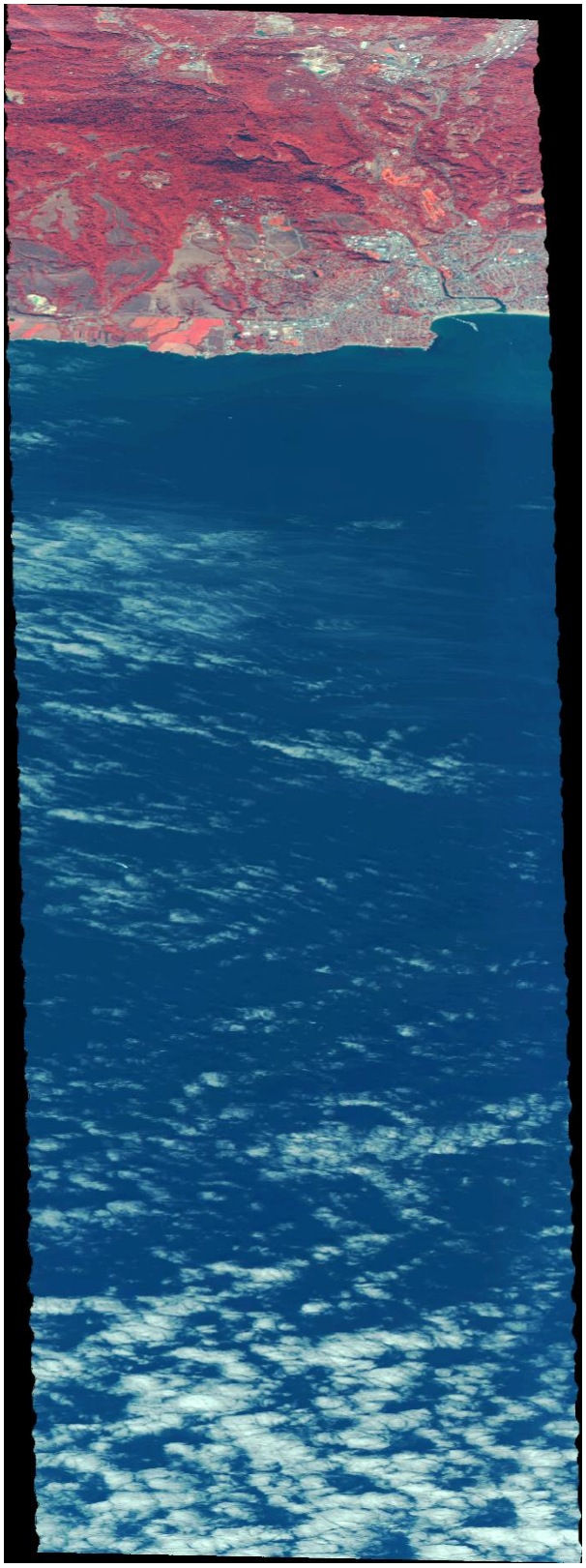

Figure 3. RGB AVIRIS image taken on 29 October, 2008 between 20:10 and 20:19 GMT, over the west coast of the northern California.

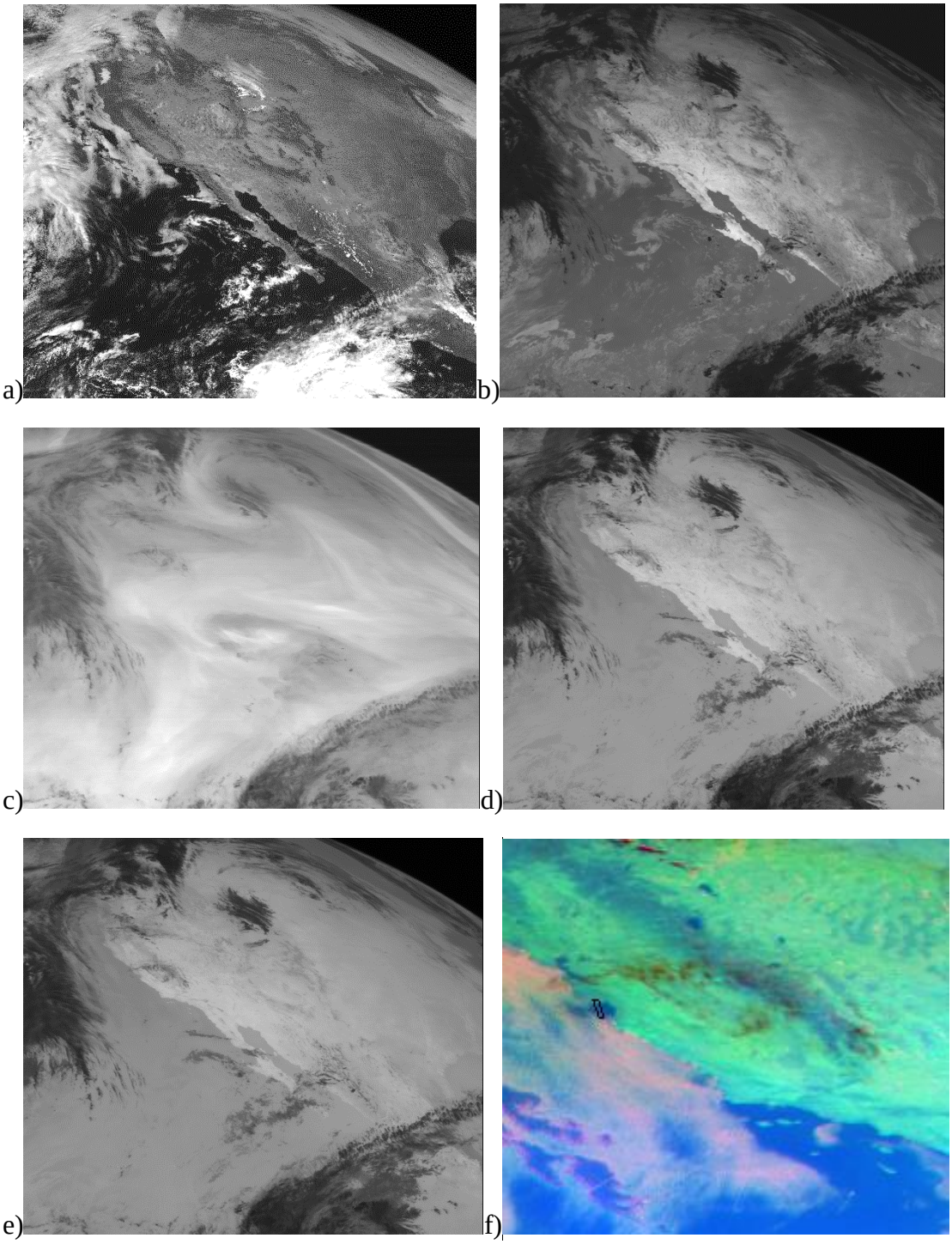

Figure 4. GOES-11 images taken at 20:15 GMT 29 October, 2008 over the western US showing (a) Channel 1, (b) Channel 2, (c) Channel 3, (d) Channel 4, (e) Channel 5, and (f) a false color composite focused on the area of interest (black lines highlight the spatial coverage of the AVIRIS data, and pink, blue, and aquamarine colors represent cloud, ocean, and land areas respectively).

Despite the fact that AVIRIS has been in operation since 1987, very little cloud detection work using these data has been published. To date, only one study (Gao et al.,1990) has attempted to cloud-screen AVIRIS data using the ratio of measured reflectance of the water vapor absorbing channels (0.94 and 1.14 μm) over measured reflectance at an atmospheric window channel (1.04 μm). However, the Gao et al. (1990) method, based on the differences in water vapor absorptions between cloudy and clear regions, can still misidentify near-surface clouds as cloud free regions. In this study, by better utilizing observations from a total of 224 spectral channels, a new threshold-based cloud screening method has been developed for AVIRIS data. The method is developed by studying the spectral behaviors of clouds and other ground features over the entire AVIRIS spectrum. Thresholds are selected to distinguish cloudy regions from clear regions using observations from cloud sensitive channels. To determine these thresholds, multiple training samples were hand-selected from cloud free regions including ocean, city, grass-land (green vegetation), and forest pixels (Fig. 5). City pixels were picked from four different areas. Vegetation pixels were from visible grassland areas. Two forest pixels were picked from visibly dark and bright forest areas respectively. Besides these cloud free pixels, over-water cloud pixels (for low clouds) were selected from both optically thin and thick cumulus clouds. An optically thick cloud pixel was taken from a bright cloudy region, while an optically thin pixel was taken near a cloud edge, as it has a relatively low albedo value. It is noted that cloud optical depth is proportional to the reflectance at the visible spectrum (e.g., King et al. 1998). Also, thin cirrus clouds were found at the northeast side of the image and were selected for this study for comparison purposes.

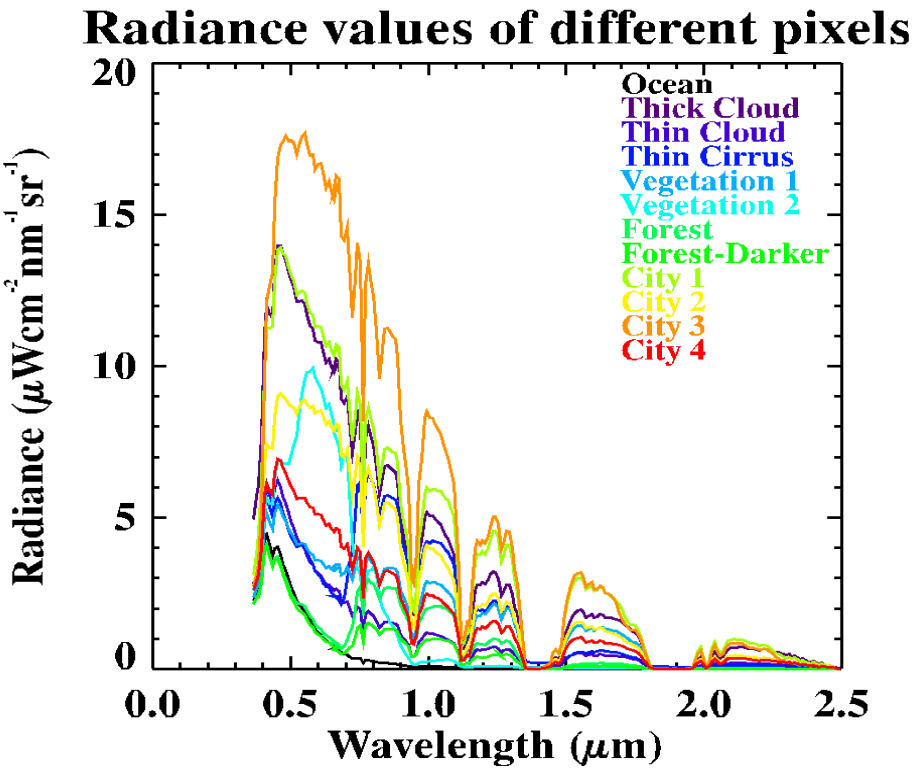

Figure 5. All training pixels and their radiance values across the whole spectrum.

Due to the large amount of information in Fig. 5, the spectral responses of water cloud, cloud-free forest and cloud-free ocean pixels are highlighted in Fig. 6. As seen in Figs. 5 and 6, radiance values from water pixels approach to zero at wavelengths greater than approximately 1.4 μm. In addition, radiances of water pixels around the 2.28 μm channel are lower than other surface features (Fig. 5). Therefore, the 2.28 μm channel was used to identify water pixels, and regions with radiance values lower than 0.03 μW cm^{-2} nm^{-1} sr^{-1} at this channel are considered to be ocean/water pixels (Fig. 7b). However, some dark forest features are also identified as water pixels as shown in Fig. 7b. Therefore, an additional threshold test that uses radiance values from the 0.8 μm channel where high reflectance values from the vegetated areas are expected was implemented

(threshold value of 0.5 µW cm^{-2} nm^{-1} sr^{-1}). The combined 0.8 and 2.28 µm channels threshold tests work well and enable water pixel identification as shown in Fig. 7c.

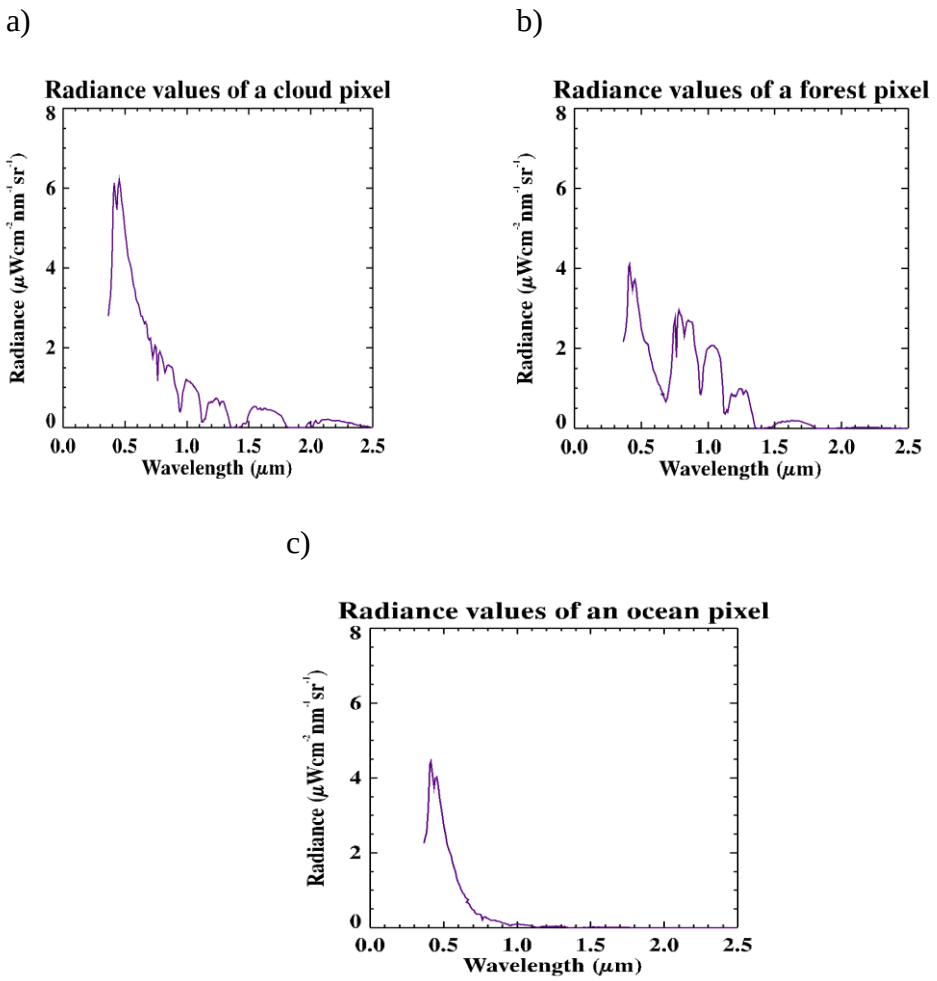

Figure 6. Selected cloud, forest and ocean pixels and their respective radiance values throughout the AVIRIS spectrum.

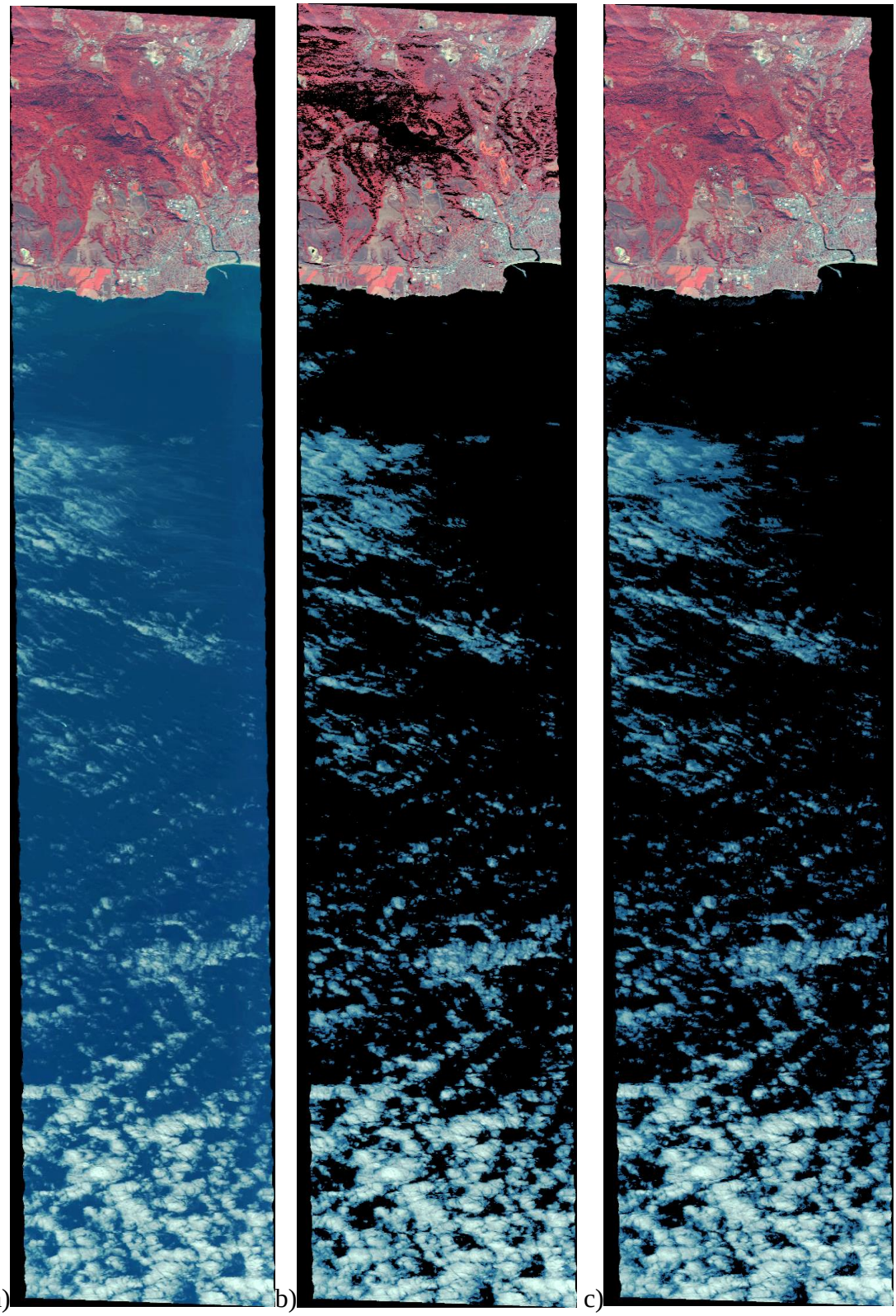

Figure 7. (a) AVIRIS original image, (b) water-mask after the 2.28 μm channel test, and (c) water-mask after using both the 0.8 and 2.28 μm channel tests (black color indicates water).

In the next step, vegetative areas are detected and removed. The ratio of the 0.88 and 0.67 μm channels was used to identify vegetative regions. A threshold value of 0.8 was chosen after a series of sensitivity tests. As shown in Fig. 8b, the vegetation test successfully labels vegetative regions, leaving the urban regions undetected. Also, sensitivity tests suggest that ratios among various channels can be used to identify urban regions. The ratio of radiances between 0.55 and 0.48 μm channels, with a threshold value of 0.92 (Fig. 9b), and the ratio of radiances between 0.65 and 0.45 μm channels, with a threshold value of 0.8 (Fig. 9c) were selected for this purpose. Additionally, a thin cirrus test was developed using the 1.38 μm channel. The optimum threshold was found to be 0.125 μW cm^{-2} nm^{-1} sr^{-1}, as shown in Fig. 8c. Note that the use of the 1.38 μm channel for detecting thin cirrus clouds is not new, as it has been implemented for standard cirrus cloud detection with MODIS (Ackerman et al., 2010). Non-cloudy pixels can still go undetected after applying all the tests listed above (Fig. 10b), especially over cities. Therefore, the spectral responses of urban areas were checked with the use of AVIRIS data as shown in Fig. 11. Clearly, signals from the city and cumulus cloud pixels are similar at all spectral channels ranging from 0.4 to 2.5 μm. Thus, it is difficult to discriminate city from water cloud pixels using AVIRIS data alone.

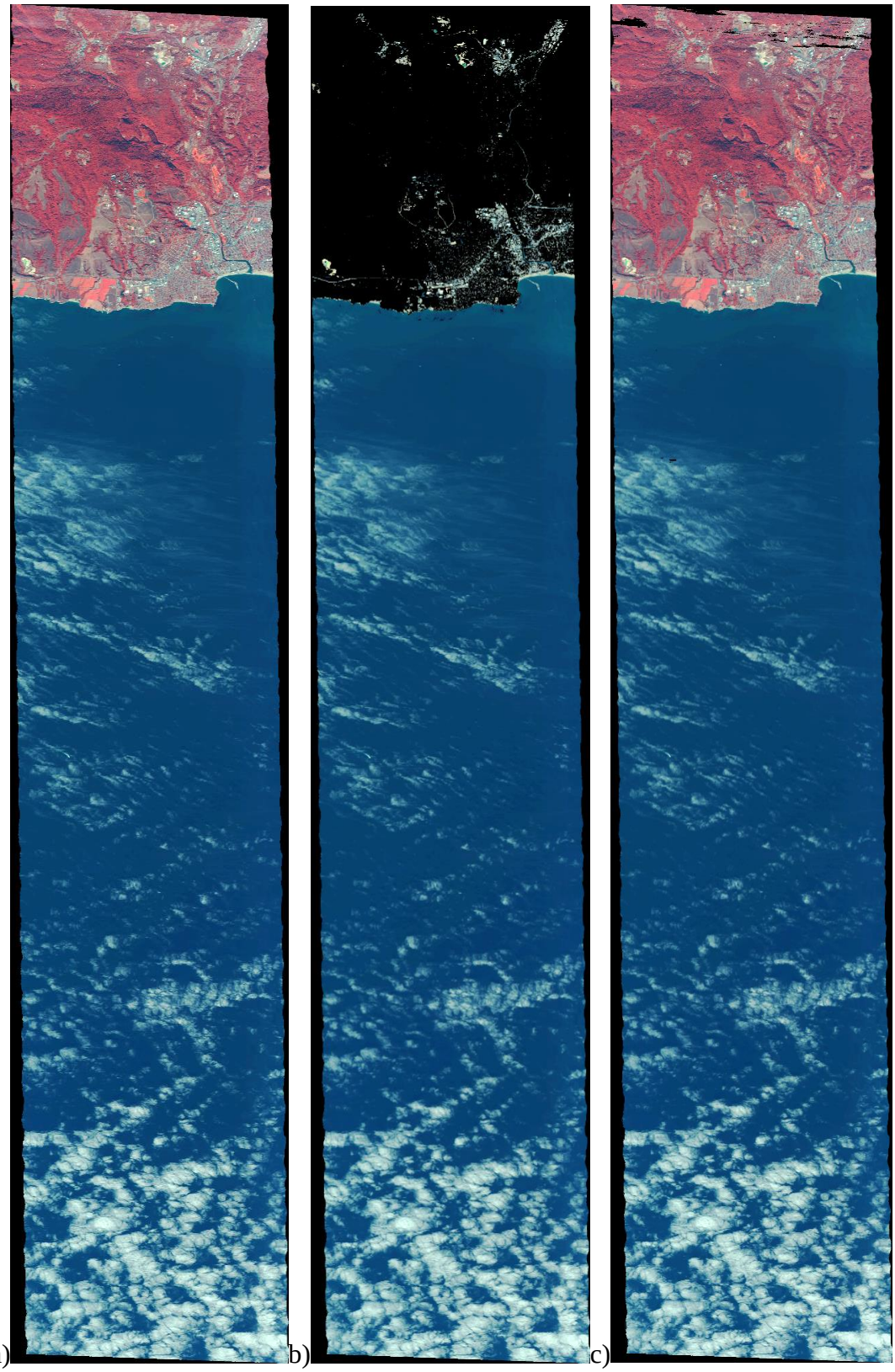

a) b) c)

Figure 8. (a) AVIRIS original image, (b) vegetation mask, and (c) thin cirrus mask (black color indicates vegetation in (b) and thin cirrus in (c)).

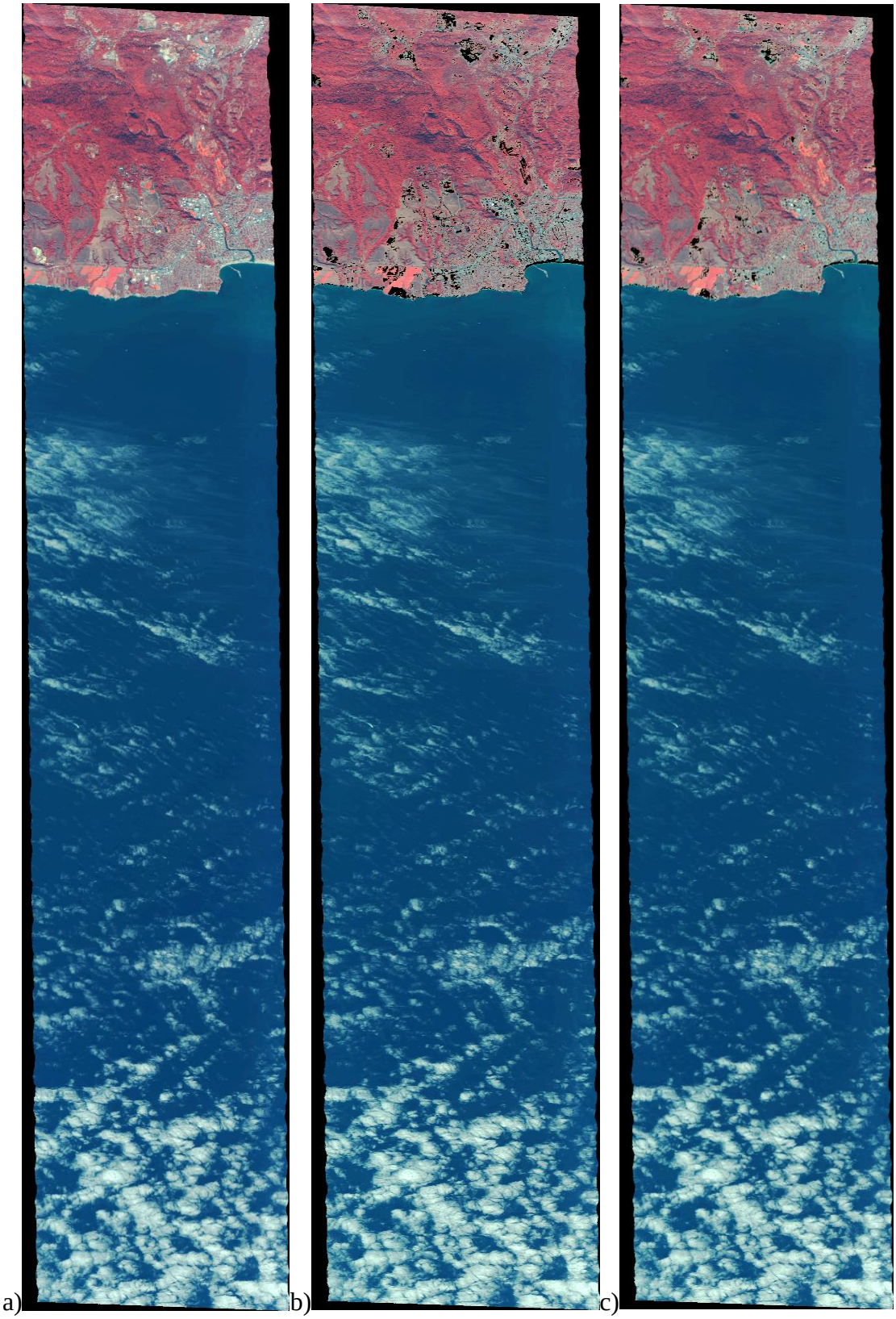

Figure 9. (a) Original AVIRIS image and (b and c) the results of two enhancing tests (black color indicates masked areas by tests).

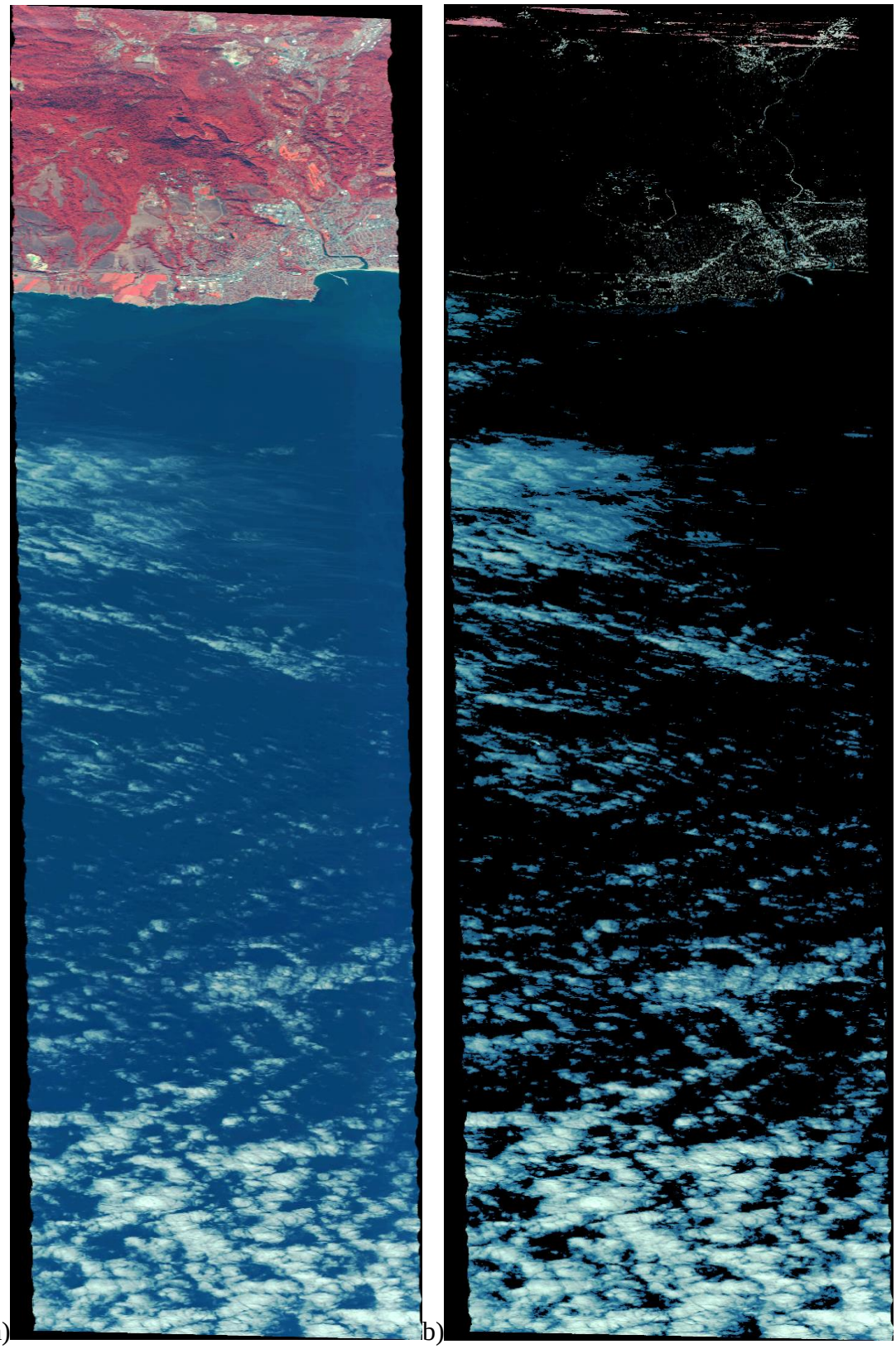

Figure 10. (a) Original AVIRIS image and (b) result of the combination of all tests (black color indicates masked areas by tests and purple color indicates thin cirrus).

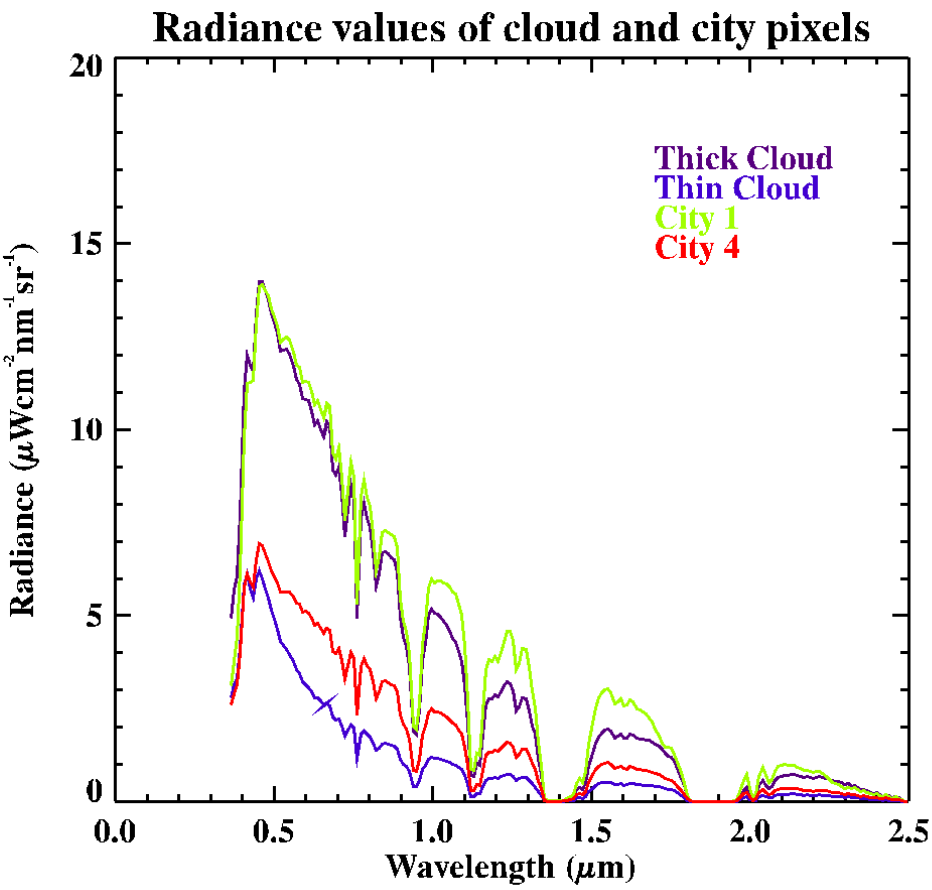

Figure 11. Spectral responses of selected cloud and city pixels for the spectral range from 0.4 to 2.5 μm.

Attempts were also made to locate spectral ranges that can be used to discriminate cities from cumulus clouds using the first and/or second derivative of the radiance values estimated from AVIRIS. Figure 12 shows the first derivative of the radiance values with respect to wavelength for selected city and water cloud pixels. Figure 13 shows a similar plot, but the second derivative. As this figures indicate, no spectral range is present that could be used to separate city from water cloud pixels. As suggested from this study, water cloud and city pixels are spectrally similar within the AVIRIS spectrum. It is difficult, if not impossible, to discriminate cities from cumulus clouds using observations at the visible, near IR and shortwave IR channels.

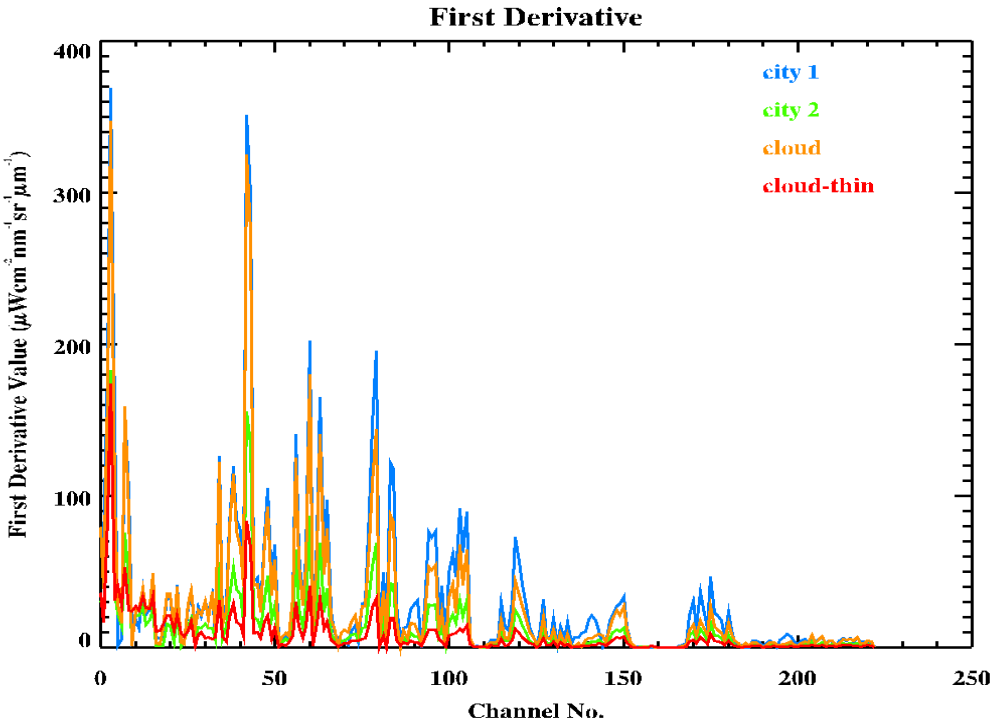

Figure 12. First derivative of radiance values respect to the wavelength.

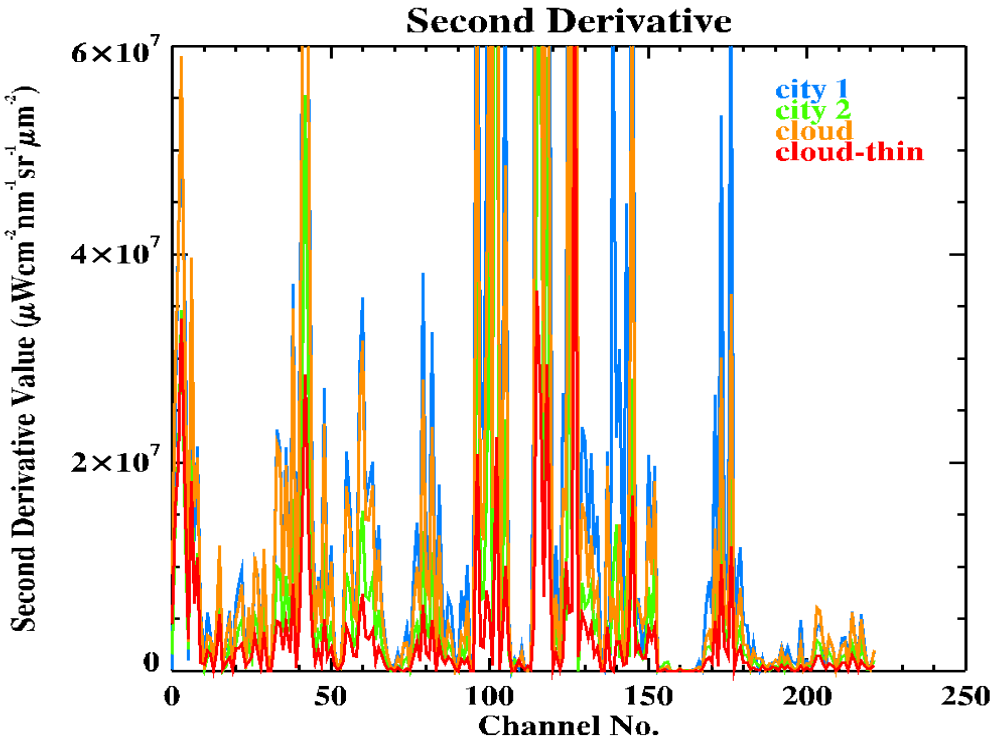

Figure 13. Second derivative of radiance values respect to the wavelength.

Due to the fact that the cloud detection scheme developed in this study is not fully able to distinguish city from water cloud pixels, the focus hereinafter is on over-water clouds. Land pixels are removed from the study based on their geo-locations. Figure 14b shows the enhanced cloudy features, as detected from the cloud screening method discussed above, with the actual clouds shown in white. Figure 14c is similar to Figure 14b, with all land pixels masked. The resulting dataset as shown in Figure 14c is used for inter-comparisons with GOES data.

Regarding GOES data screening, the Jedlovec and Laws (2003) method (the BTH cloud detection algorithm) is used to identify cloudy areas in the IR spectrum. First, differences in temperatures between the GOES 3.9 μm and 10.7 μm channels ($\Delta T_{10.7\text{-}3.9}$) are computed (Fig. 15b). As shown in Fig. 15b, clouds are darker than cloud-free pixels. In Figure 15b, these dark areas denote large negative values of $\Delta T_{10.7\text{-}3.9}$, and the differences are more apparent for over-water than over-land clouds.

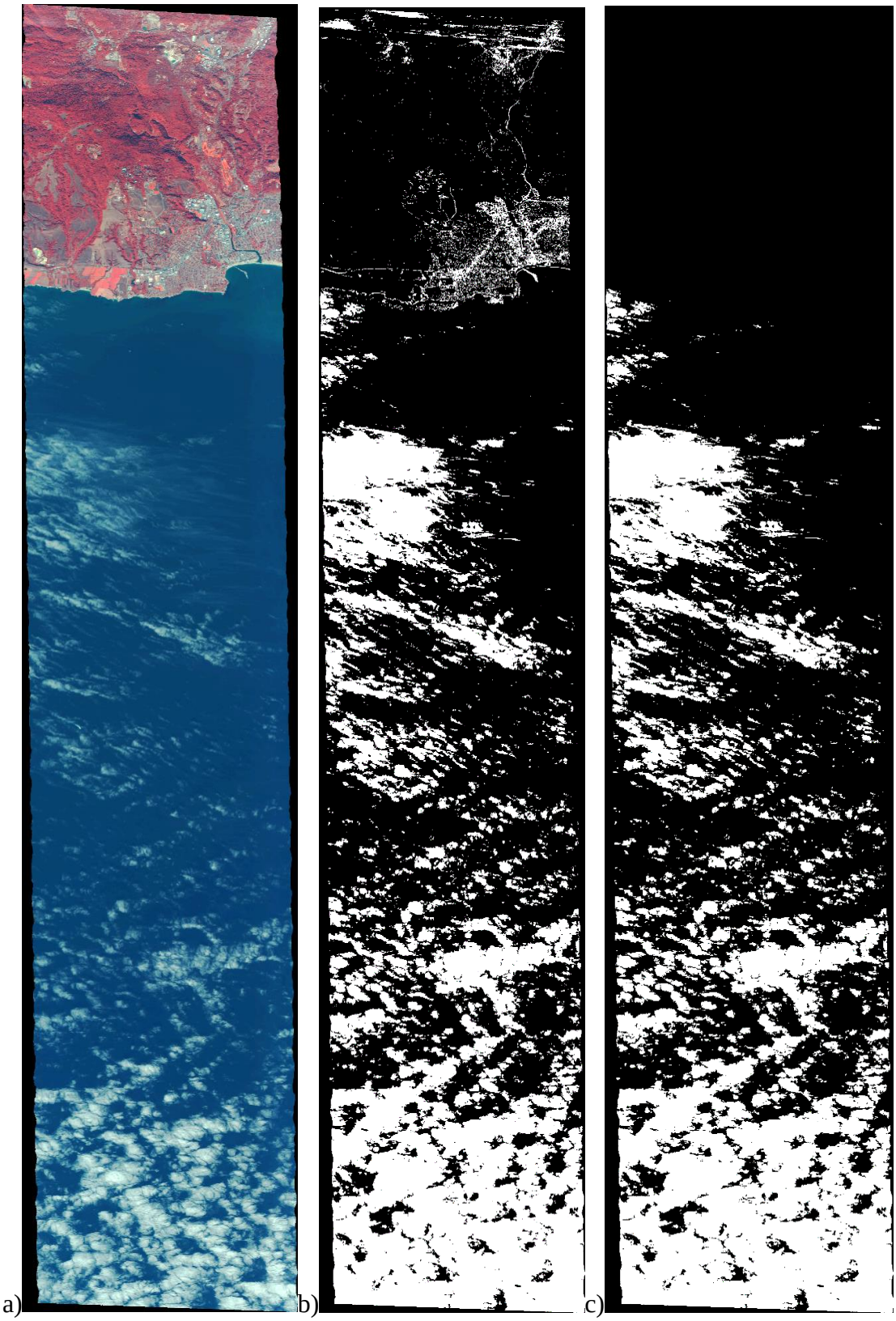

Figure 14. (a) Original AVIRIS image, (b) black and white image showing cloudy, and non-cloudy areas, and (c) application of the land-mask to this image.

a) 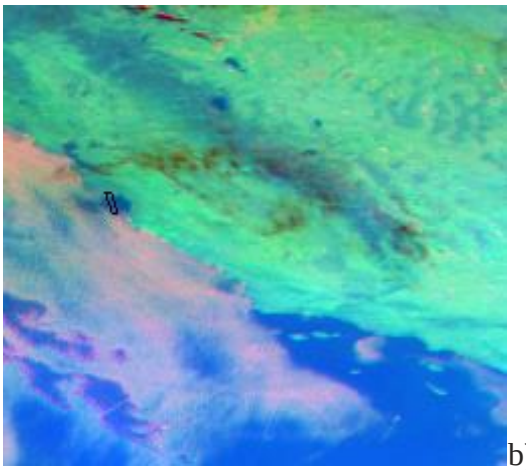 b) 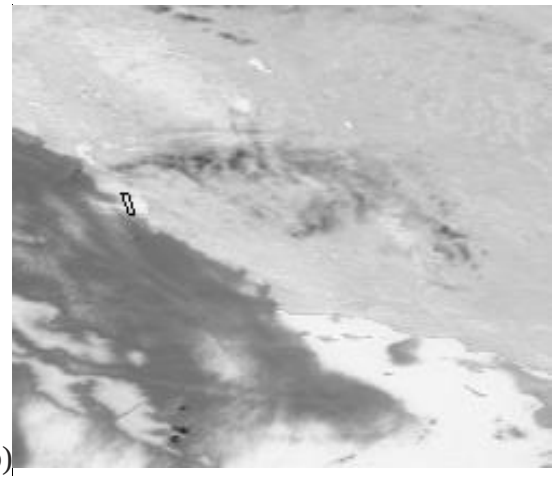

Figure 15. (a) Original false color GOES and (b) corresponding $\Delta T_{10.7\text{-}3.9}$ images (black lines highlight the spatial coverage of the AVIRIS data).

The first step of the BTH algorithm attempts to determine cloud edges. According to Jedlovec and Laws (2003), the temperature differences of the two adjacent pixels ((i) and (i-1)) have to be > 27.2 K in order to mark pixel (i) as cloudy. In this study, this threshold did not work effectively because most of the temperature differences are smaller than this threshold. A later study using the BTH algorithm (Haines et al., 2004), suggests a better adjacent pixel test that is based on the variance between two pixels. According to their results, the variance value has to be greater than 7.2 K. This threshold was used, and the resulting image (Fig. 16a) shows that a significant portion of cloud edges are detected.

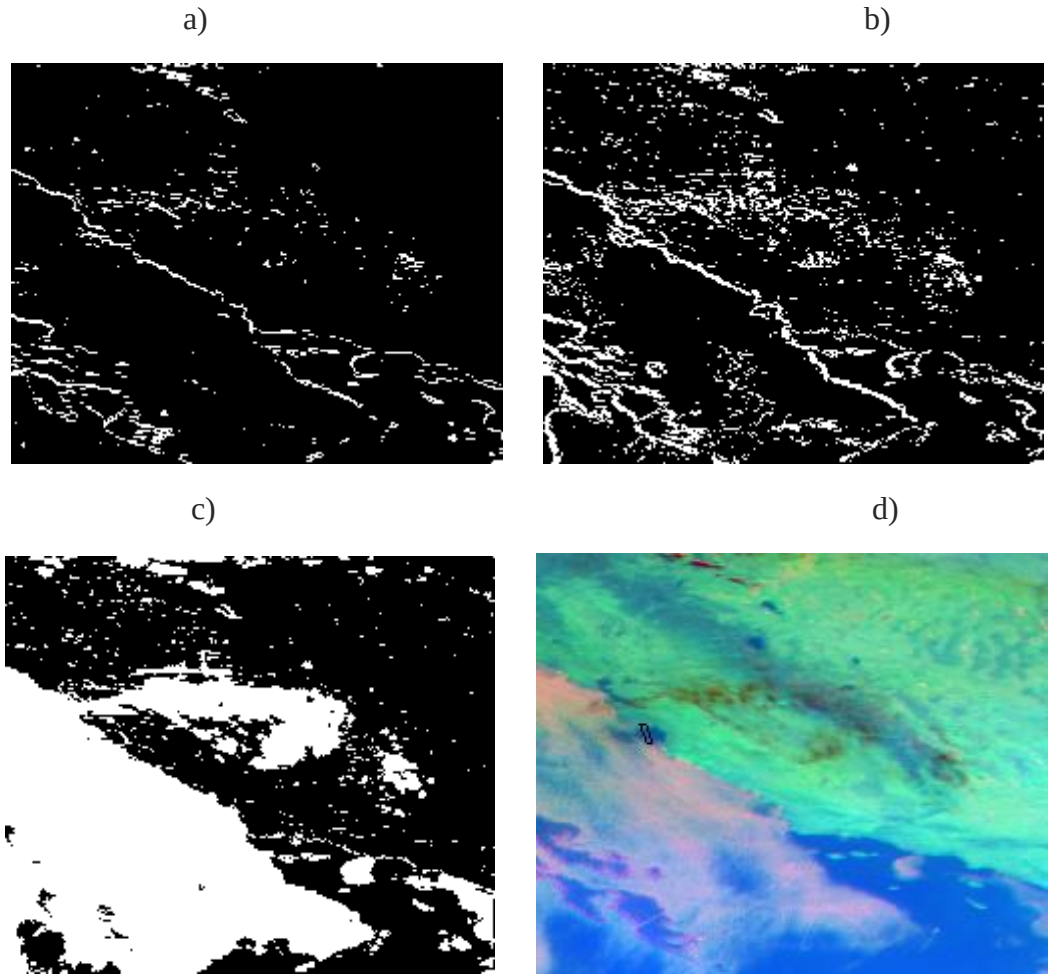

Figure 16. Results of the (a) first step, (b) second step, and (c) all steps of the BTH algorithm, and (d) original false color GOES image (black lines highlight the spatial coverage of the AVIRIS data).

The second step of the BTH algorithm determines how pixels that are within cloud edges are further labeled as clouds. If a pixel (i-1) is marked as cloudy, the $\Delta T_{10.7-3.9}$ value of i – (i-1) has to be less than 0 K. Furthermore, for the pixels that are marked as clear, the $\Delta T_{10.7-3.9}$ values have to be less than -3.1 K or greater than 2 K. The application of this step is shown in Fig. 16b and in comparison to Fig. 16a, more cloud edges are detected when both the first and the second steps are implemented.

As mentioned earlier, the last two steps in the BTH method detect clouds in regions where the first two steps fail. According to Jedlovec and Laws (2003), thresholds

for the third step are -5.1 K for pixels having negative $\Delta T_{10.7-3}$ values and 2 K for positive $\Delta T_{10.7-3}$ values. To implement these thresholds, multi-day composites are constructed using GOES-11 data at the same observing time from a total of 20 days of data. Again, the thresholds provided by Haines et al. (2004) were used, as the thresholds listed in Jedlovec and Laws (2003) produced poorer results. Thresholds of -4.0 K and 2.5 K were used for pixels with negative and positive values of $\Delta T_{10.7-3.9}$, respectively, and the resulting image is shown in Fig. 16c. The last step is an IR threshold test, where the highest temperatures from the 10.7 μm channel--estimated using a 20-day composite--are compared to the observed temperatures from the GOES-11 10.7 μm channel. The goal of this step is to detect clouds that are missed by the previous three steps. Herein, the threshold from Jedlovec and Laws (2003) was used, as this threshold has not changed. However, no additional cloud pixels were detected in this step. Figure 16c, which labels cloudy features as white and the remaining features as black, shows the result of the GOES cloud detection using the four steps mentioned above.

The BTH method does not include observations from the GOES visible channel, possibly because the GOES visible and IR channels have different spatial resolutions. For comparison purposes, clouds were also identified using a visible channel data based method on the GOES cloud detection method described by Jedlovec et al. (2009). They used a GOES albedo threshold of 25% over land and 7% over ocean for masking cloudy GOES pixels. Based on sensitivity studies, the optimum threshold was found to be 5.5% for over-ocean cloud detection in this study. It is believed that this lower threshold is a result of signal degradation in the GOES visible channel (e.g., Zhang et al. 2001).

A total of 629 GOES-11 ~1×1 km (at the visible channel) pixels, which are located within the AVIRIS overpass as shown in Fig. 17a, were selected for this study. Figure 17b shows the resulting image after applying the 5.5% threshold for the visible channel. Note that the threshold is validated through visual inspection of the GOES visible image. However, as shown in Fig. 17a, it is indeed difficult to select a fixed threshold for GOES cloud detection, as cloudy and cloud free pixels are hard to define even with 1 km data. Therefore, lowering or raising the threshold results in either over- or under-detection of the cloud fields. Nevertheless, sensitivity is illustrated by varying the threshold. The resulting images for varying thresholds are shown in Fig. 17c for a threshold value of 4.5% and Figure 17d for a threshold value of 7.0%. Results clearly show that more (less) areas are detected as cloudy by lowering (raising) the threshold, indicating the difficulties in accurately defining the cloud field through satellite remote sensing.

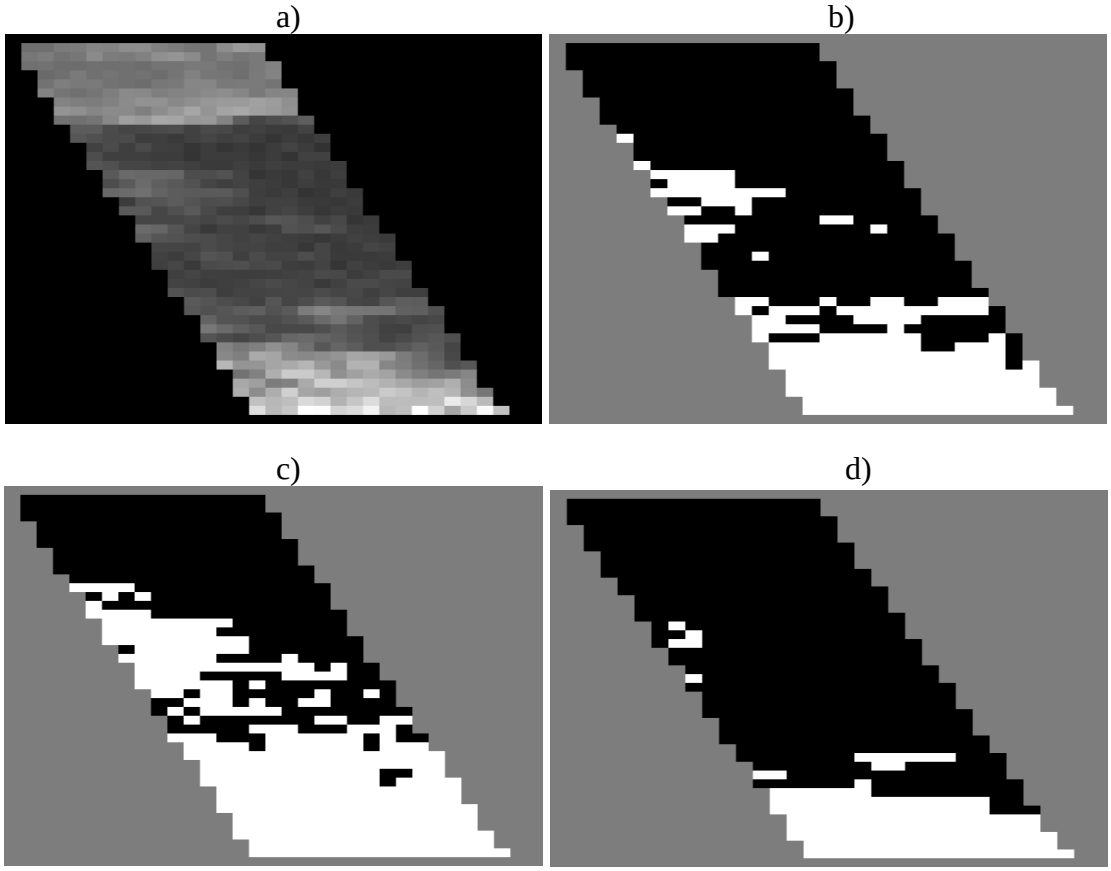

Figure 17. (a) GOES channel 1 image in the AVIRIS scan area and the detected cloudy GOES pixels (white color) using thresholds of (b) 5.5%, (c) 4.5%, and (d) 7.0%.

Comparison of GOES IR and Visible Cloud Detection Methods

The AVIRIS granule covers an area of approximately 9 km × 58 km. Shown in Fig. 18a are the collocated GOES pixels at the 3.9 μm channel relative to the AVIRIS scan. A total of 38 collocated 4 km resolution GOES pixels were located within the AVIRIS overpass. This result is not unexpected, as the spacing of GOES-11 infrared data is 4 km, while AVIRIS data spacing is 11.5 m. Similarly, Fig. 18b shows the collocated GOES pixels at the visible channel, after degrading from 1 km to 4 km data spacing. In order to degrade the 1 km visible data to 4 km, geometric averages were applied.

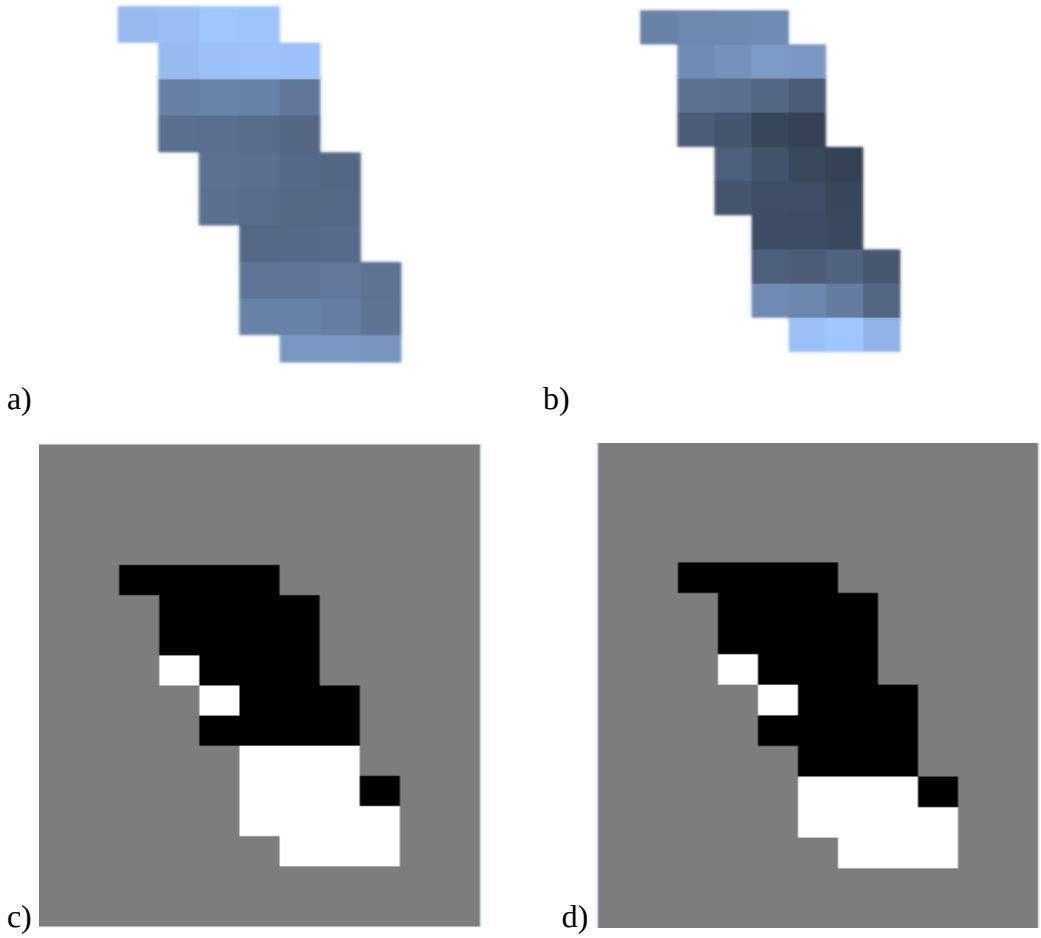

Figure 18. (a) GOES pixels from Channel 2 in the AVIRIS scan area, (b) degraded Channel 1 pixels in that area, (c) resulting image after applying the BTH method, and (d) resulting image after applying the albedo method.

Figures 18c and 18d show detected cloudy pixels (in white) based on the BTH and the visible albedo methods, respectively. In general, cloudy fields detected from the two methods are similar; both picked the cloudy region at the bottom of the image as well as two cloudy regions in the middle of the image. However, three more GOES pixels (4 km resolution) are selected as cloudy pixels based on the BTH method. These three pixels are found to be around cloud edges after visually inspecting both AVIRIS and GOES images. The three GOES pixels, marked as cloudy pixels in the second step of the BTH method, have low albedo values in the visible channel. Though attempts to adjust the visible

threshold were made, a perfect match of cloudy regions was not obtained. Figure 18 highlights the existing problem currently faced by cloud detection studies.

Comparison of GOES and AVIRIS Cloud Fraction

As shown in Fig. 18c, 15 of the 38 collocated GOES pixels are detected as cloudy pixels based on the BTH cloud screening method. The real cloud fraction within the GOES footprint, however, can be studied using collocated AVIRIS data that have a spatial resolution of 11.5 m. As shown in Fig. 19, a cloudy GOES pixel, as detected by the GOES cloud screening method, has only 44% cloud cover (56% sub-pixel clear-sky contamination) on average, as determined from AVIRIS data. The remaining cloud free GOES pixels as detected by the GOES cloud screening scheme have nearly 19% cloud residuals (or sub-pixel cloud contamination). Note that this study focuses on over-ocean cloud detection. Thus, 12 out of 38 GOES pixels are removed as these pixels are located over land.

A similar study is also attempted for the GOES cloud fields using the GOES visible channel. A total of 629 1 km spacing GOES pixels were within the AVIRIS granule. Of those 629 pixels, 193 of them were located over land and were thus excluded from further analysis. Even at the 1 km spacing, a GOES cloudy pixel, as identified based on the GOES visible-based cloud screening method, has only 64% cloud cover on average as suggested from collocated AVIRIS data, while 17% of the GOES detected cloud free regions are contaminated with various cloud types (Fig. 20). Even though only one AVIRIS granule is used in this study, this study suggests that both sub-pixel cloud and clear-sky contamination exist for satellite data such as GOES.

The impacts of sub-pixel clouds on GOES observed radiances and temperatures were also examined. Figure 21 shows a scatter plot of GOES Channel 1 radiance versus cloud fraction, as determined from the AVIRIS data for GOES detected cloud free pixels. The mean radiance value for cloud-free ocean regions agreed by GOES and AVIRIS is 2.04 μW cm^{-2} nm^{-1} sr^{-1}, while the average radiance value for all detected GOES cloud-free ocean regions is 2.31 μW cm^{-2} nm^{-1} sr^{-1}. Thus, sub-pixel cloud contamination introduced a 13% increase in cloud-free GOES Channel 1 radiance values for this case. Naturally, sub-pixel contamination can also impact atmospheric property retrievals, such as aerosol retrievals that use GOES visible channel data.

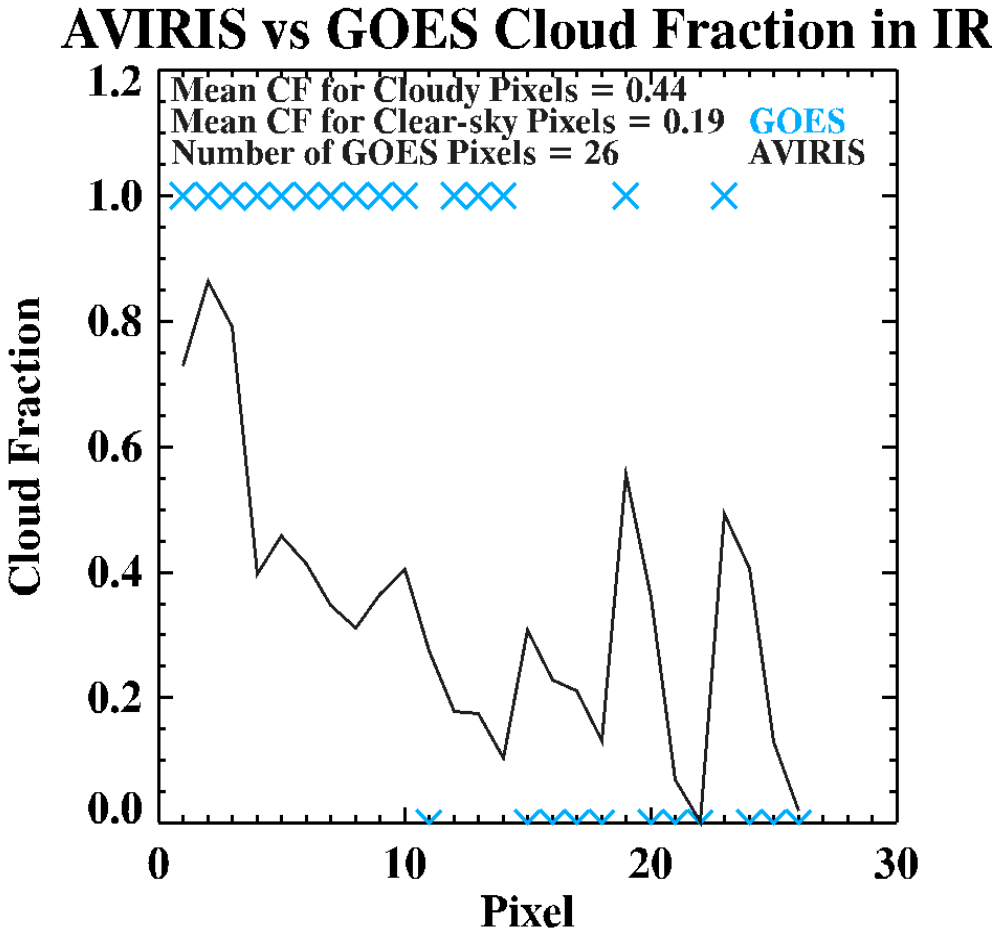

Figure 19. Comparison of the percentage of the cloudy areas in the infrared region.

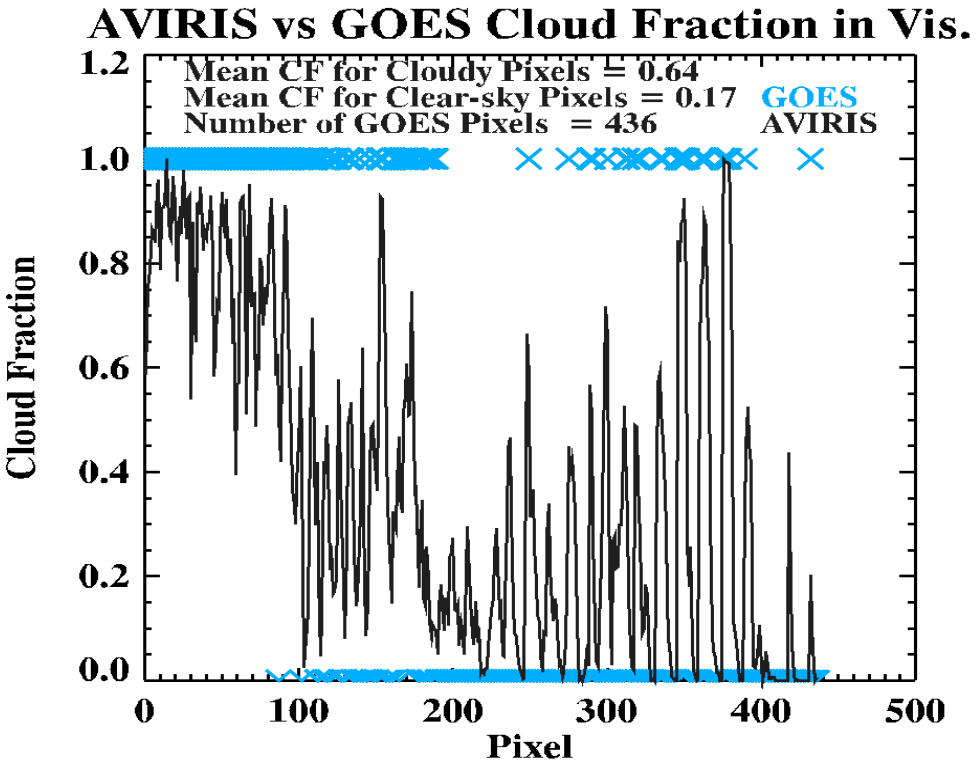

Figure 20. Comparison of the percentage of the cloudy areas in the visible region

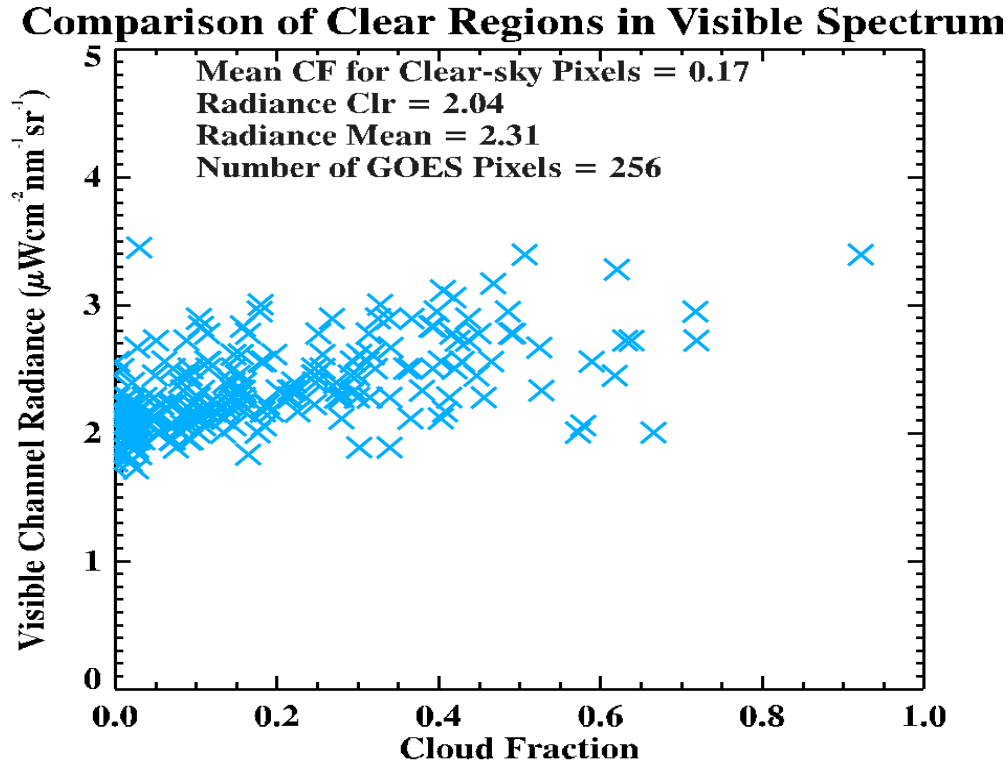

Figure 21. GOES visible radiance as a function of AVIRIS cloud fraction, for GOES detected cloud free regions.

Table 7. Effect of sub-pixel cloud/clear-sky contamination in measured GOES radiance (Rad.) and temperature (Temp.) values. (Radiance values are in μW cm^{-2} nm^{-1} sr^{-1} and temperature values are in Kelvin, and percentages in parenthesis after values represent increases/decreases in value).

Channel Number	1 4.5% Thres. (Rad.)	1 5.5% Thres. (Rad.)	1 7.0% Thres. (Rad.)	2 (Temp.)	3 (Temp.)	4 (Temp.)	5 (Temp.)
Change in Cloudy Pixel values of GOES	-2.02 (35%)	-1.27 (22%)	-0.77 (12%)	-4.91	-0.86	-0.91	-0.85
Change in Clear Pixel values of GOES	0.11 (5%)	0.27 (13%)	0.41 (20%)	0.98	0.35	0.75	0.65

Table 7 shows the impacts of sub-pixel cloud/clear-sky contamination for all GOES channels. For the visible channel, a 22% reduction in GOES radiance exists in GOES cloudy regions (using an albedo threshold value of 5.5%), which could potentially impact cloud optical property retrievals. Results for different threshold values are provided in Table 7 to show the effects of use of different thresholds on radiance values. By varying the cloud screening threshold from 5.5% to 4.5% and 7.0%, an average of ±10% variation in the reduction is found in cloudy pixels. For GOES IR channels, ~0.8-0.9 K variations are found for GOES Channels 3-5 over the cloudy regions, while the largest temperature increase of ~5 K is at GOES Channel 2 and owes to sub-pixel clear sky contamination. This large difference may largely due to the contamination from the solar energy at the 3.9 μm channel. Over GOES detected cloud free regions, a 2-11% increase in Channel 1 radiance values occurs with a varying albedo threshold value of 4.5-7%. For the GOES IR channels, IR temperature variations of 0.3-1 K occur for various channels due to sub-pixel cloud contamination.

The maximum AVIRIS cloud fraction is 89% for GOES cloudy pixels detected using the BTH method. Thus, the temperature values for GOES pixels with this AVIRIS cloud fraction are used as the temperature values for the fully cloudy case. Again, although only one AVIRIS data granule is used, this case study suggests that both sub-pixel cloud and clear-sky contamination can be significant over regions with stratocumulus clouds and should be taken into consideration in future cloud as well as other atmospheric property retrievals that utilize measurements from passive sensors such as GOES and MODIS.

Uncertainty Analysis

There are a few sources of uncertainty in this study. First, cloud systems move with time. In this study, nearly coincident AVIRIS and GOES data have been selected. The overpass time of the AVIRIS data is between 20:10 and 20:19 GMT on 29 October, 2008, while the estimated GOES scan time over the study area is 20:17 GMT of the same day. Still, it is necessary to check if there are observable movements in the cloud fields. Therefore, the visible and IR cloud screening methods have been applied to the GOES data that are obtained 15 minutes before (20:00 GMT) and after (20:30 GMT) the study period (Fig. 22). Changes in the cloudy fields are observable but are not drastic, indicating that the cloud system is relatively stable during the study period.

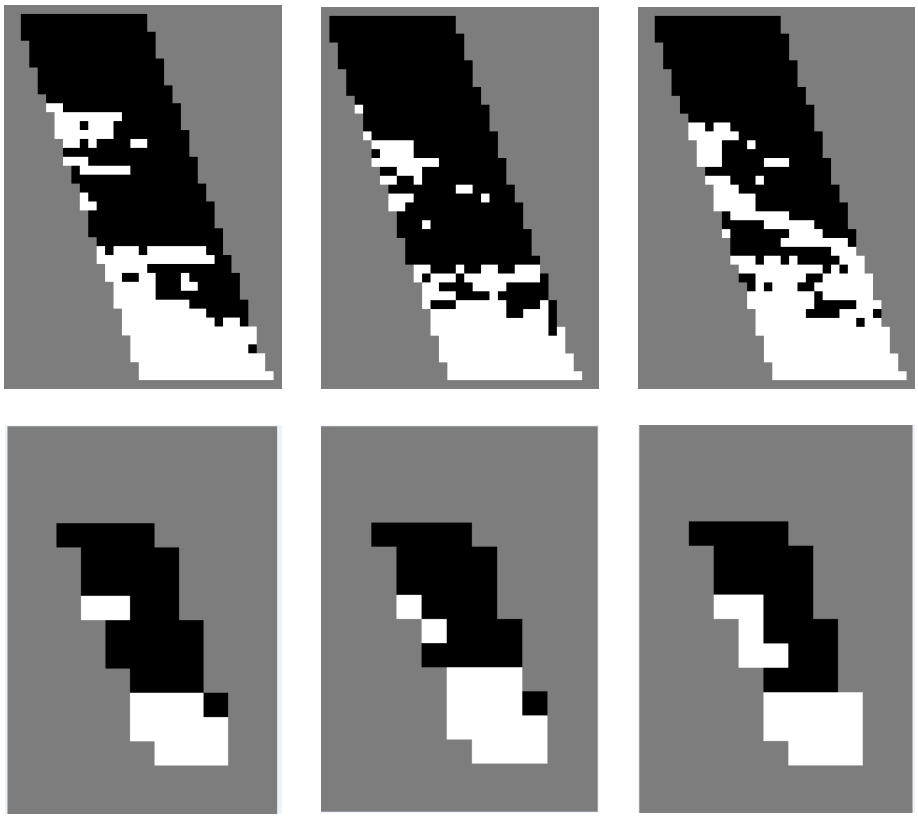

Figure 22. Visible channel cloud mask (upper row) and infrared channels cloud mask (lower row) for GOES data from 20:00, 20:15, and 20:30 GMT, on 29 October, 2008 (from left to right, respectively).

Second, geo-location and navigation errors (on the order of 1 visible pixel) for GOES need to be accounted for. Consequently, an experiment has been designed to consider both issues. In this experiment, four simulated GOES (visible) datasets are created. They are constructed by shifting the original GOES data one column to the left and right, and one row up and down. The simulated datasets are created to mimic the movements of the cloud fields as well as geometric calibration errors. The previous analysis is then repeated with the shifted data. Table 8 shows the sub-pixel cloud and clear-sky contamination in the four simulated GOES datasets. Slight variations occur for both the sub-pixel cloud contamination (57-66%) and sub-pixel clear-sky contamination (16-19%), suggesting that the results of this study are robust.

Table 8. Sub-pixel cloud and clear-sky contamination for four simulated GOES datasets. The four GOES datasets were created by arbitrarily shifting the GOES pixels one pixel away from their original location, either to the left or to the right, or up or down.

	Original Pixel Location	Move the image up by one row	Move the image down by one row	Shift the image to the right by one column	Shift the image to the left by one column
Cloudy Areas	64%	66%	57%	65%	62%
Clear Areas	17%	19%	19%	19%	16%

Modeled and observed radiance values at the AVIRIS spectrum

As an exploratory study for evaluating the potential of utilizing AVIRIS data in atmospheric aerosol studies, modeled radiance values from SBDART and measured radiance values from AVIRIS were compared. An over-water cloud free pixel is randomly chosen from the AVIRIS data. The modeled and measured radiance values for the selected over-water pixel are then compared. The focus is on over-water simulations, as surface albedo models can drastically vary over land. To correctly model the observed scenes, the viewing geometry such as solar zenith, viewing zenith, and satellite and solar azimuth angles, as well as geo-location of satellite overpasses are used as input into the radiative transfer model. Since no observed near surface wind speed data and atmospheric profile are available, default values from the SBDART model were used for those parameters. Default aerosol models (rural, oceanic, urban, and tropospheric aerosol models) included in SBDART were also used to test sensitivity to varying aerosol optical depths (AOD).

Figure 23 shows the comparison between SBDART and AVIRIS radiance values for the chosen ocean pixel. Although the differences between modeled radiance values from SBDART and observed radiance values from AVIRIS values are small for the

spectral channels above 0.7 μm, the differences are evident for wavelengths shorter than 0.7 μm. It is believed that the differences are introduced through use of an inaccurate ocean surface reflectance model used in the SBDART RTM. Other factors such as the near surface wind speed and calibration of the AVIRIS data may also contribute to these differences. However, it is still possible to study the relative sensitivity of each spectral channel to changes in aerosol type and aerosol loading. For this purpose, aerosol type and concentration (as a function of AOD) were varied to investigate the potential of using AVIRIS data for aerosol studies. For this sensitivity study, four aerosol models that are included in SBDART are used. The four aerosol models are rural, ocean, urban, and tropospheric aerosol models. In addition, the aerosol loading was altered through the use of AOD values of 0.1, 0.2 and 0.5. At a first glance, large increases in radiance values occur in channels 0.50, 1.00, 1.24, 1.55 and 2.04 μm owing to varying aerosol optical depth from 0 to 0.5 in all models. This indicates that these spectral channels are the most sensitive to the presence of aerosol plumes.

To be more specific, Fig. 24 shows changes in radiance values with aerosol type when using a constant aerosol optical depth value of 0.5. At the spectral range of 0.4-1.0 μm, urban aerosols can be easily separated from other types of aerosols as a result of their spectral responses, with the optimal channels for separating aerosol types actually being around 1.0-1.5 μm. In this spectral range, tropospheric, oceanic and urban aerosols have their own distinct spectral responses and can thus be separated. Figure 24 is a typical example of how RTM calculations can be used for assisting algorithm development for satellite aerosol studies.

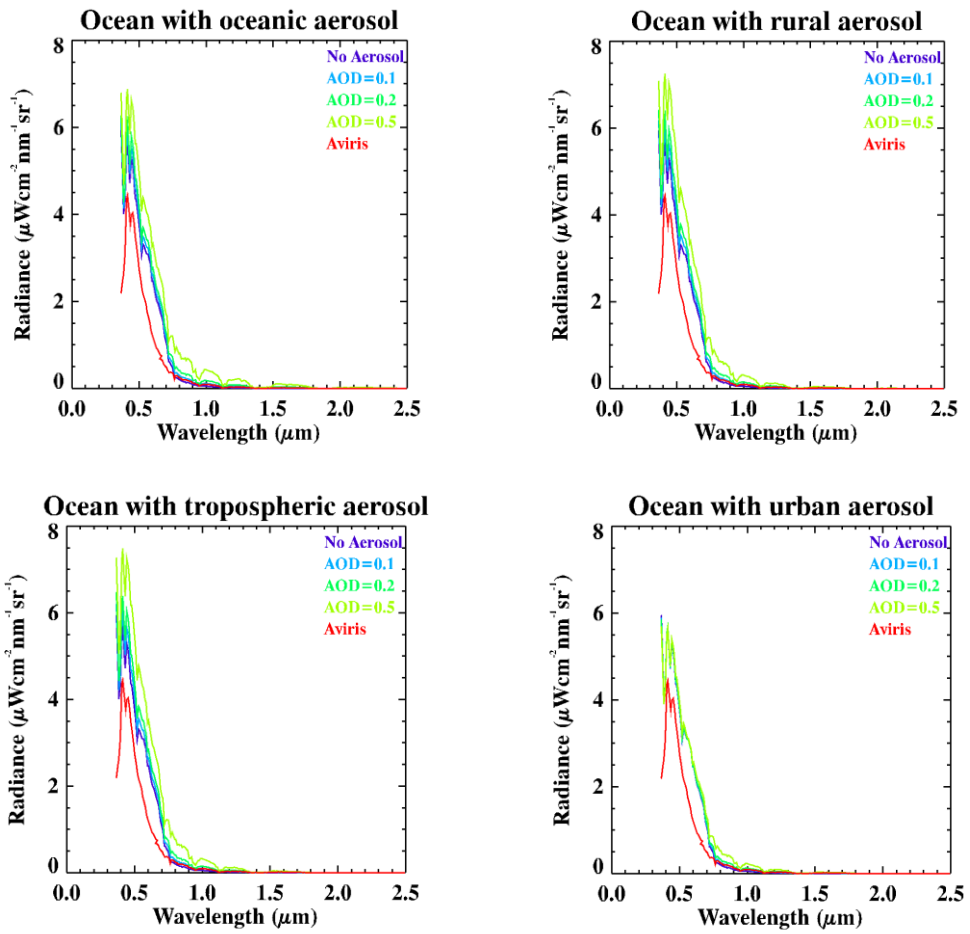

Figure 23. AVIRIS and SBDART comparison over ocean for different types of aerosols (AVIRIS data are shown in red, and SBDART outputs are shown in purple, blue, green, and yellow for AOD=0, 0.1, 0.2, and 0.5, respectively).

Spectral responses in the water vapor and oxygen absorption channels were also examined by fixing aerosol type and varying aerosol optical depth. Figure 25 shows changes in simulated AVIRIS radiance at the 0.72 nm water vapor absorption band (e.g., Lacis and Hansen 1974), as well the oxygen A-band (~0.76 μm). Spectral responses for tropospheric aerosols at the oxygen and water vapor absorbing channels are clearly different from that between 0.72 and 0.76 μm. Assuming an oceanic aerosol model, the results are similar for the water vapor channels of 0.9 and 1.2 μm, and the spectral

responses of aerosols at the wavelengths between these two channels, as indicated by Fig. 26. Such information can be explored in future studies of aerosol property retrievals.

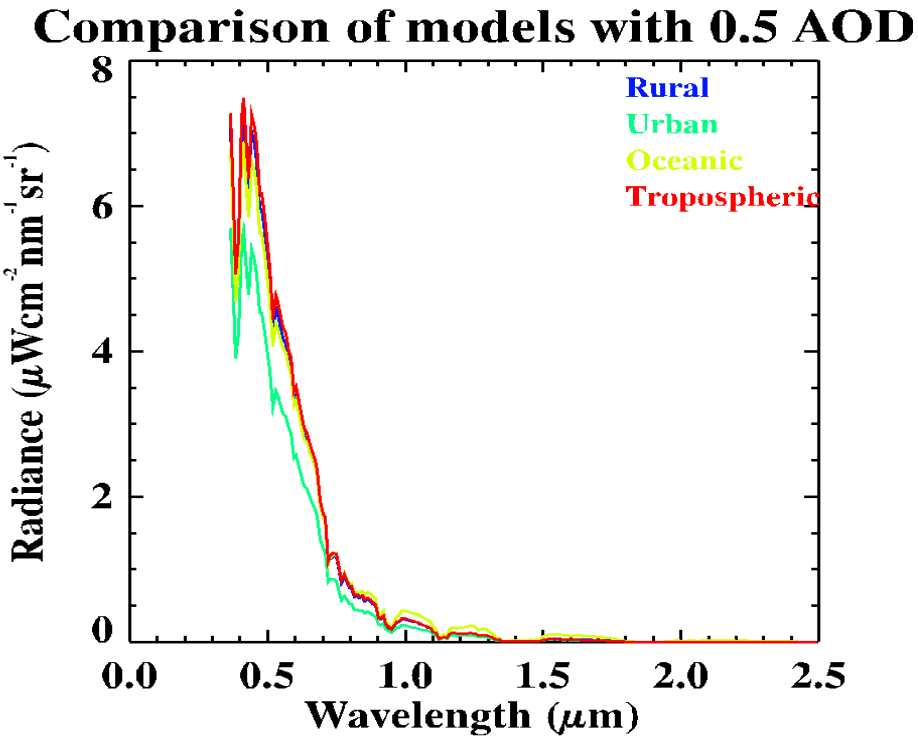

Figure 24. Radiance values for different aerosol models throughout the spectrum for an AOD of 0.5.

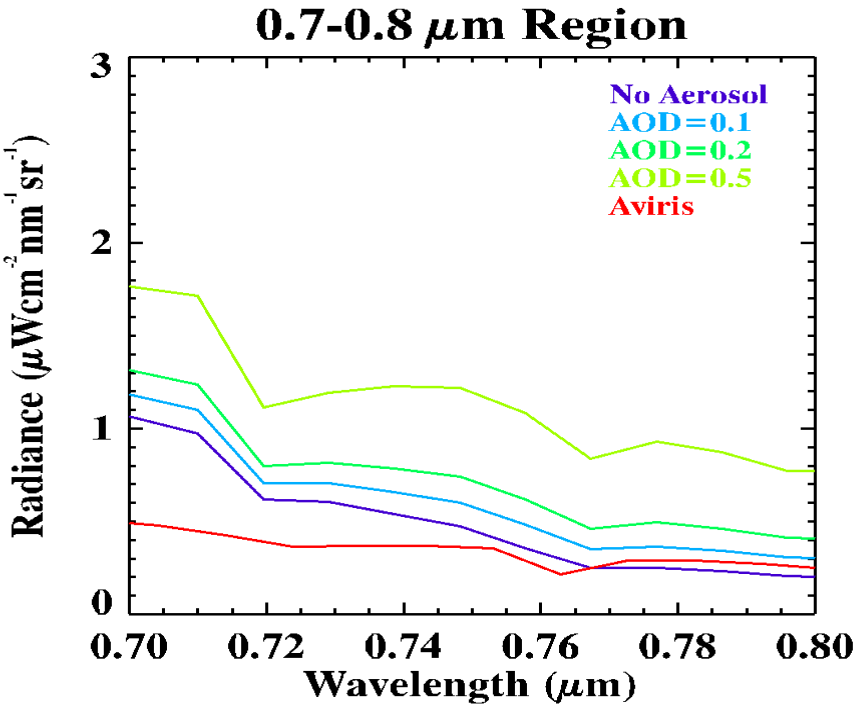

Figure 25. Change in radiance values between the 0.7 and 0.8 μm channels with varying AOD when the tropospheric aerosol model is used.

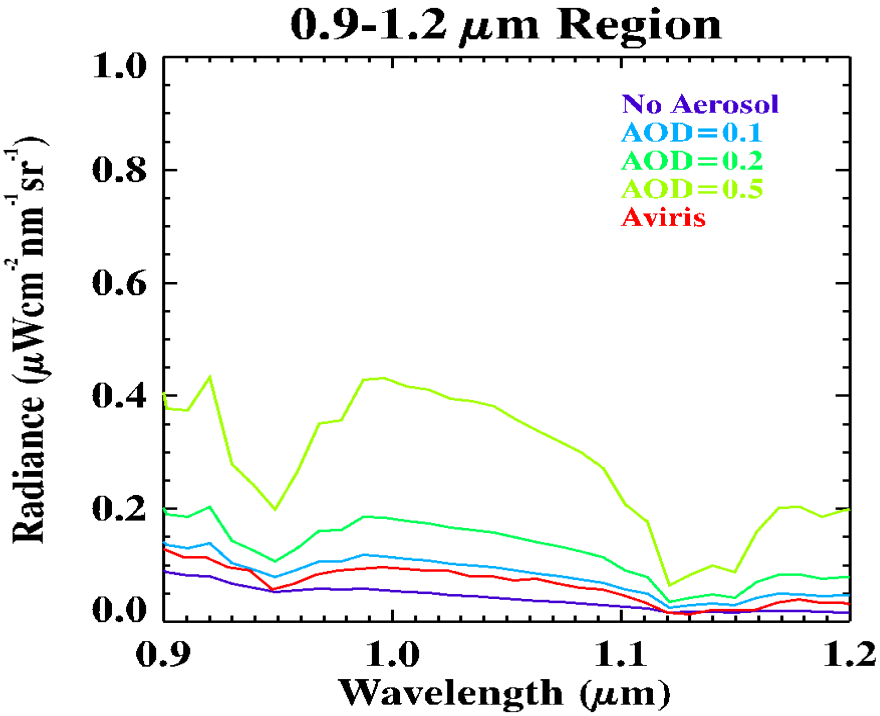

Figure 26. Change in radiance values between 0.9 and 1.2 μm channels with varying AOD when the oceanic aerosol model is used.

CHAPTER IV

SUMMARY AND CONCLUSIONS

Sub-pixel cloud/clear-sky contamination in GOES imagery data are studied using collocated Airborne Visible/Infrared Imaging Spectrometer (AVIRIS) and Geostationary Operational Environmental Satellite (GOES-11) datasets over the Monterey Bay, California region (~ 36.55-37º N and 122.1-122º W). This work shows that cloud/clear-sky pixels detected with satellites have a significant amount of sub-pixel clear-sky/cloud contamination, which may affect the accuracy of satellite-based retrievals. Clouds are identified using AVIRIS data by developing a new cloud detection algorithm that is based on the exclusion of non-cloudy scenes, while GOES-based cloud detection is accomplished using the bi-spectral threshold and height (BTH) method (e.g., Jedlovec and Laws 2003) and an albedo threshold method. Moreover, Santa Barbara Discrete ordinate method (DISORT) Atmospheric Radiative Transfer (SBDART) model results are compared to AVIRIS radiance values to evaluate the potential for using AVIRIS data in aerosol studies.

AVIRIS data for various surface types are analyzed for developing a new threshold-based cloud detection algorithm. This algorithm uses specific channel values and ratios based upon the spectral responses of various features within the AVIRIS spectral domain. Even though the threshold based method is capable of masking clouds over oceans and most land surfaces, it fails over cities. This is possibly due to clouds and cities having similar spectral characteristics over the range of 0.4-2.5 μm. Additional

channels from the thermal IR region are needed to discriminate clouds from cities. Also, one could compute spatial derivatives to discriminate large clouds from cities. Therefore, only over-water AVIRIS data are used in cloud comparisons.

Through the use of two different methods, GOES data are analyzed to identify cloudy areas. The BTH method is used for detecting clouds through the use of the 4 km infrared channels, while the albedo method is used for the 1 km visible channel. This is because the BTH method uses temperature values, while the albedo method uses reflectance (albedo) values. These two methods are compared to determine whether they detect the same cloudy/clear-sky pixels. By degrading the spatial resolution of the visible channel, this comparison is performed at 4 km data spacing. Differences between the two methods are found around cloud edges, which further suggests that the BTH method cannot accurately determine cloudy areas around cloud edges.

To determine real cloud fraction in the GOES data through the use of AVIRIS data, pixels from the GOES visible channel and infrared channels are collocated with the 11.5 m spaced AVIRIS pixels. This collocation is performed using the geo-coordinates of each pixel. Cloud residuals in GOES clear-sky areas are found to be the same for the two cloud screening methods. However, clear sky contamination in GOES cloudy areas is found to be higher for the BTH cloud screening method, which uses observations from the IR channels. This finding suggests that clear sky contamination (in cloudy areas) has a larger influence on coarse resolution satellite data, although this could be because of the algorithm or the nature of the data.

Since sub-pixel cloud/clear-sky contamination can affect radiance/temperature values, radiance/temperature values of GOES clear and cloudy areas are further

investigated to determine the magnitude of this effect. In the visible channel, radiance values are analyzed, while in infrared channels temperature values are analyzed. Impacts of both sub-pixel cloud and clear-sky contamination are found to be less than 1 K for the IR channels for most cases. However, a ~5 K change is found at the GOES 3.9 μm channel due to sub-pixel clear-sky contamination, largely related to the contamination from solar energy. Similarly, significant sub-pixel cloud and clear-sky contaminations are found in the GOES visible channel. Clearly, both sub-pixel cloud and clear-sky contamination need to be accounted for when obtaining atmospheric property retrievals using GOES data.

To explore the potential use of AVIRIS data in aerosol studies, a radiative transfer modeling study was completed. Through the use of a radiative transfer model (SBDART), the sensitivity of AVIRIS radiance values to changes in over-water aerosol properties was studied. Measured AVIRIS radiance values for an ocean pixel are inter-compared with the simulated AVIRIS radiance values using SBDART. In general, modeled and measured radiance values agree over most of the AVIRIS spectral range, yet differences are observable, especially in channels that are less affected by absorption. This is possibly due to inaccuracies in the surface reflectance model used in the calculations. The sensitivity of AVIRIS data to aerosol properties is studied by varying both aerosol type and aerosol optical depth in SBDART simulations. Although a few spectral channels that are most sensitive to changes in aerosol loading were identified, potential for studying aerosol features at absorbing channels, such as the oxygen A-band, is not discounted. Still, aerosol studies using AVIRIS data is an ongoing topic that deserves further exploration.

It is concluded that satellites having coarser spatial resolution may misidentify clouds as clear regions or incorrectly assign clear regions as cloudy scenes. This sub-pixel cloud/clear-sky contamination may cause uncertainties in cloud and other atmospheric property retrievals. However, only one AVIRIS granule is used in this study, as AVIRIS data are not generally to the scientific community. A study like this that includes additional hyper-spectral data should be conducted. Also, the potential benefits of using hyper-spectral data in aerosol studies are still unknown. A study of aerosols that utilizes hyper-spectral data sets should be performed to test the feasibility of performing aerosol retrievals using both oxygen and water vapor absorbing channels, and the channels that are identified herein as being sensitive to the presence of aerosol plumes.

APPENDIX

Appendix A

Acronyms and Definitions

AOD	Aerosol Optical Depth
AVIRIS	Airborne Visible/Infrared Imaging Spectrometer
BIP	Band Interleaved by Pixel
BTH	Bi-spectral Threshold and Height
CW	Clock-Wise
DEM	Digital Elevation Model
DISORT	Discrete Ordinate Radiative Transfer
DN	Data Number
DOD	Department of Defense
FWHM	Full Width at Half Maximum
GLT	Geometric Look-up Table
GMT	Greenwich Mean Time
GOES	Geostationary Operational Environmental Satellite
GVAR	GOES Variable
IR	Infrared
JPL	Jet Propulsion Laboratory
K	Kelvin
LEO	Low Earth Orbiting
MODIS	Moderate Resolution Imaging Spectroradiometer
MTI	Multispectral Thermal Imager
NAD	North America Datum
NASA	National Aeronautics and Space Administration
NOAA	National Oceanic and Atmospheric Administration
RMS	Root Mean Square
RTM	Radiative Transfer Model
SBDART	Santa Barbara DISORT Atmospheric Radiative Transfer
SRF	Spectral Response Function
UTM	Universal Transverse Mercator
WGS	World Geodetic System

REFERENCES

Ackerman, S., R. Frey, K. Strabala, Y.Liu, L. Gumley, B. Baum, P. Menzel (2010), Discriminating clear-sky from cloud with MODIS: Algorithm theoretical basis document (MOD35) version 6.1, Report, Univ. of Wis., Madison.

AVIRIS overview (2013). Retrieved November 2, 2013 from http://aviris .jpl.nasa.gov/aviris/index.html.

Brubaker, N. J., G. Jedlovec (2004), A cloud maskfor AIRS, 13th Conference on Satellite Meteorology and Oceanography, Norfolk, Virginia.

Chrien, T. G., Green, R. O., Chovit, C., and Hajek, P. (1995b), New calibration techniques for the Airborne Visible/Infrared Imaging Spectrometer (AVIRIS). In Summaries of the Fifth Annual JPL Airborne Earth Science Workshop, JPL Publ. 95–1, Vol. 1, Jet Propulsion Laboratory, Pasadena, CA, pp 33–34.

Chrien,T. G., Green, R. O., Sarture, C. M., Chovit, C., East-wood, M. L., and Eng, B. T. (1993), Airborne Visible/Infra-red Imaging Spectrometer (AVIRIS): recent improvements to the sensor. In Summaries of the Fourth Annual JPL Air-borne Geoscience Workshop, JPL Publ. 93–26, Vol. 1, Jet Propulsion Laboratory, Pasadena, CA, pp. 27–30.

Cylhek P, Borel C, Davis A B, Augustine J and Hodges G, (2004), Effect of broken clouds on satellite-based columnar water vapor retrieval, IEEE Geosc. Remote Sens., Lett, 1, 175–8.

Evans, K. F., R. P. Lawson, P. Zmarzly, D. O'Connor, and W. J. Wiscombe (2003), In situ cloud sensing with multiple scattering lidar: Simulations and demonstration. J. Atmos. Oceanic Technol., 20**,** 1505–1522.

Gao, B. C., and Goetz, A. F. H. (1990), Determination of a cloud area from AVIRIS data. In Proceedings of the Second Airborne Visible/Infrared Imaging Spectrometer (AVIRIS) Workshop, JPL Publ. 90–54, Jet Propulsion Laboratory, Pasadena, CA, pp. 157–161.

GOES Imager Instrument (2013). Retrieved November 2, 2013 from http://noaasis .noaa.gov/NOAASIS/ml/imager.html.

GOES N Series Data Book (2009). Retrieved November 2, 2013 from http://goes.gsfc .nasa.gov/text/GOES-N_Databook_RevC/Databook_RevC.pdf

GOES Sounder Instrument (2013). Retrieved November 2, 2013 from http://noaasis .noaa.gov/NOAASIS/ml/sounder.html.

Green, R., Eastwood, M. L., & Williams, O. (1998), Imaging spectroscopy and the airborne visible/infrared imaging spectrometer (AVIRIS), Remote Sensing of the Environment, 65, 227-248.

Haines, S. L., R. J. Suggs, and G. J. Jedlovec (2004), The Geostationary Operational Environmental Satellite (GOES) product generation system, NASA Tech. Memo., NASA TM-2004-213286.

Hawkinson, J. A., W. Feltz, and S. A. Ackerman (2005), A comparison of GOES sounder- and cloud lidar- and radar-retrieved cloud-top heights, J. Appl. Meteorol., 44, 1234– 1242.

Henderson, B. G., and P. Chylek (2005), The effect of spatial resolution on satellite aerosol optical depth retrieval, IEEE Trans. Geosci. Remote Sens., 43(9), 1984–1990.

IPCC, (2011), In: Edenhofer, O., Pichs-Madruga, R., Sokona, Y., Seyboth, K., Matschoss, P., Kadner, S., Zwickel, T., Eickemeier, P., Hansen, G., Schlömer, S., von Stechow, C. (Eds.), IPCC Special Report on Renewable Energy Sources and Climate Change Mitigation. Cambridge University Press, Cambridge, United Kingdom/New York, NY, USA.

Jedlovec, G. J. and Laws, K. (2003), GOES cloud detection at the Global Hydrology and Climate Center. Preprints, 12th Conference on Satellite Meteorology and Oceanography, Long Beach, CA, USA, Am. Meteor. Soc., P1.21.

Jedlovec, G. (2009), Automated detection of clouds in satellite imagery. Advances in Geoscience and Remote Sensing, 303–316.

King, M., S.-C. Tsay, S. Platnick, M. Wang, and K.-N. Liou (1998), Cloud retrieval algorithms for MODIS: Optical thickness, effective particle radius, and thermodynamic phase, Algorithm Theor. Basis Doc. ATBDMOD-05, NASA Goddard Space Flight Cent., Greenbelt, Md.

Lacis, A. A., and J. E. Hansen. (1974), A parameterization for the absorption of solar radiation in the earth's atmosphere. J. Atmos. Sci., 31, 118–133.

Miller, M. A., G. Johannes, V. Craig, G. J. Lehenbauer, J. S. Tongue, and E. E. Clothiaux (1998), Detection of non-precipitating clouds with the WSR-88D: A theoretical and experimental survey of capabilities and limitations. Wea. Forecasting, 13**,** 1046–1062.

Morisette, J. T., Nickeson, J. E., Davis, P., Wang, Y., Tian, Y., Woodcock, C. E., et al. (2003), High spatial resolution satellite observations for validation of MODIS land products: IKONOS observations acquired under the NASA scientific data purchase, Remote Sensing of Environment, 88, 100–110.

Pierluissi J. H. and Tsai C. M. (1987), New LOWTRAN models for the uniformly mixed gases. Appl. Opt. 26, 616–618.

Ricchiazzi, P., Yang, S., Gautier, C., and Sowle, D. (1998), SBDART: A research and Teaching software tool for plane-parallel radiative transfer in the Earth's atmosphere, Bulletin of the American Meteorological Society, 79, 2101–2114.

Stamnes,K ., S.C. Tsay, W. Wiscombe, and K. Jayaweera (1988) ,Numerically stable algorithm for discrete ordinate-method radiative transfer in multiple scattering and emitting layered media, Appl. Opt., 27, 2502-2509.

Tuinder, O., R. de Winter-Sorkina, and P. Builtjes (2004), Retrieval methods of effective cloud cover for the GOME instrument: An intercomparison Atmos. Chem. Phys., 4, 255– 273.

Weinreb, M.P.,M. Jamison, N. Fulton, Y. Chen, J.X. Johnson, J. Bremer, C. Smith, and J. Baucom, (1997), Operational calibration of Geostationary Operational Environmental Satellite-8 and -9 imagers and sounders. Applied Optics, 36, pp 6895-6904.

Weinreb, M.P., D. Han, (2009), Calibration of the Visible Channels of the GOES Imagers and Sounders, NOAA NESDIS Office of Satellite Operations.

Weinreb, M.P., J.X. Johnson, D. Han, (2011), Conversion of GVAR Infrared Data to Scene Radiance or Temperature, NOAA NESDIS Office of Satellite Operations.

Zhang, J., S.A. Christopher, and B.N. Holben (2001), Intercomparison of smoke aerosol optical thickness derived from GOES 8 imager and ground-based Sun photometers, Journal of Geophysical Research: Atmospheres, Vol. 106, No. D7, 7387-7397.